ELSEVIER

Comput. Methods Appl. Mech. Engrg. 188 (2000) 363–390

Computer methods in applied mechanics and engineering

www.elsevier.com/locate/cma

Asymmetric modified spur gear drives: reduction of noise, localization of contact, simulation of meshing and stress analysis

Faydor L. Litvin [a,*], Qiming Lian [a], Alexander L. Kapelevich [b]

[a] *Department of Mechanical Engineering, Gear Research Laboratory, University of Illinois at Chicago, 842 W. Taylor Street (MC 251), 2039 Engineering Research Facility, Chicago, IL 60607-7022, USA*

[b] *Graco Inc., Minneapolis, MN, USA*

Received 26 March 1999

Abstract

An asymmetric spur gear drive is considered. The asymmetry means that larger and smaller pressure angles are applied for the driving and coast sides, respectively. The conventional design of such a drive is based on application of involute profiles. The authors propose a modified geometry of an asymmetric spur gear drive designed as a combination of an involute gear and a double crowned pinion that enables to localize and stabilize the bearing contact and obtain a favorable shape of transmission errors of reduced magnitude. Computerized design of spur gears of proposed geometry and simulation of their meshing and contact have been developed. A method of generation of a double-crowned pinion has been developed as well stress analysis of symmetric and asymmetric spur gears have been accomplished, that confirm reduction of contact and bending stresses for an asymmetric spur gear drive. The developed theory is illustrated with numerical examples.

Keywords: Asymmetric profiles; Spur gears; Modification; Simulation; Stress analysis

Nomenclature

$\alpha_i (i = \mathrm{d}, \mathrm{c})$	Pressure angles for asymmetric spur gear drive: $(i = \mathrm{d})$ for driving side profile, $(i = \mathrm{c})$ for coast side profile (Figs. 1, 2 and 7)
α_i^* $(i = \mathrm{d}, \mathrm{c})$	Profile angles for rack-cutter (Fig. 6)
ΔE, γ, λ	Errors of misalignment of center distance E, angle γ between rotational axes and lead angle λ
θ_j	Surface parameters of rack-cutter for generating of pinion $(j = \mathrm{c})$ and gear $(j = \mathrm{t})$
κ_d	Curvature of parabolic pinion rack-cutter at point Q_d (Fig. 7)
λ_t	Ratio of tooth thickness of pinion and gear measured on meshing centrodes
ν	Poisson's ratio
ρ	Radius of rack-cutter fillet (Fig. 6)
ρ_i $(i = 1, 2)$	Radius of pinion and gear centrodes being in mesh with the rack-cutter (Figs. 23 and 26)
Σ_i $(i = \mathrm{c}, \mathrm{t})$	Rack-cutter surfaces for generation of the pinion $(i = \mathrm{c})$ and the gear $(i = \mathrm{t})$
Σ_1 and Σ_2	Pinion and gear tooth surfaces being in mesh with each other

* Corresponding author. Tel.: +1-312-996-2866; fax: +1-312-413-0447.
E-mail address: FLitvin@uic.edu (F.L. Litvin).

$\Sigma_1^{(i)}$ $(i=1,2)$	Pinion tooth surface generated as envelope to rack-cutter surface $(\Sigma_1^{(1)})$, and as envelope to the surface of plunging disk $(\Sigma_1^{(2)})$
σ	Angle formed by axes x_d and x_c (Fig. 2(b))
ϕ	Generalized parameter of motion in process of meshing of pinion and gear
ψ_i	Generalized parameter of motion in process of generation of pinion $(i=1)$ and gear $(i=2)$
a	Parabola coefficient of predesigned parabolic function of transmission errors (Eq. (29))
a_c	Parabola coefficient of parabolic profile of rack-cutter (Eq. (25))
a_{pl}	Parabola coefficient of parabolic function of plunging (Fig. 8)
E, E_0	Initial and current shortest center distances in generation by a plunging disk (Fig. 8)
FE, FEA	Finite element, finite element analysis
L_d	The magnitude of distance from point Q_d to point P in Fig. 7
l_D	Displacement of disk in translation in direction parallel to the pinion axis (Fig. 8)
l_d	The magnitude of distance from point B to point M in Fig. 6
$\mathbf{M}_{ji}, \mathbf{L}_{ji}$	Matrices 4×4 and 3×3 for transformation from S_i to S_j of point coordinates and projections of vectors
N_i	Number of teeth of the pinion $(i=1)$ and the gear $(i=2)$
$\mathbf{N}_i$	Normals to the surfaces of rack-cutters or disk represented in coordinate system S_i $(i=a, c, D, e, t)$
$\mathbf{n}_f^{(i)}$	Unit normals to the pinion $(i=1)$ and gear $(i=2)$ tooth surfaces represented in the fixed coordinate system
P, P^*	Diametral pitch of the gear drive (P), generating rack-cutter (P^*)
P–P	Instantaneous axis of rotation
r_a, r_p, r_{bi}	Radii of addendum circle, pitch circle , and base circles for driving side $(i=d)$ and coast side $(i=c)$ profiles (Figs. 2–4)
r_{bp}, r_{bg}	Radii of base circles of pinion and gear being in mesh (Fig. 5)
$\mathbf{r}_i(u_c, \theta_c)$	Position vector of parabolic rack-cutter surface represented in coordinate system S_i $(i=a, c)$
S_i	Designation of i coordinate system
s_i $(i=p, g)$	Tooth thickness of the pinion $(i=p)$ or the gear $(i=g)$ measured along the centrodes (Eq. (1))
$\mathbf{v}_D^{(D1)}$	Vector of relative velocity of the plunging disk with respect to the pinion represented in coordinate system S_D
w_k	Width of space of the pinion $(k=p)$ and gear $(k=g)$ rack-cutters measured on centrodes (see Eqs. (2) and (3))

1. Introduction

Asymmetric spur gear drives was the subject of research accomplished previously in [5.8]. Unlike the version of asymmetric spur gear drives represented in [5], a larger pressure angle for the driving side but not for the coast one has been proposed in [8]. The detailed geometry of asymmetric spur gears has been represented in [8].

New developments of asymmetric spur gear drives (with a larger pressure angle for the driving side) are represented in this paper. The contents of the paper cover:

1. Basic geometric relations for an asymmetric spur gear drive with a larger pressure angle for the driving side.
2. Modification of pinion geometry that enables: (i) to reduce the level of transmission errors and provide a more favorable shape for the function of transmission errors, and (ii) localize and stabilize the bearing contact.
3. Computerized simulation of meshing and contact of a misaligned gear drive by application of developed Tooth Contact Analysis (TCA) computer program.

4. Determination of contact and bending stress and comparison with the stresses determined for a symmetric spur gear drive. It is proven that an asymmetric gear drive enables to reduce the stresses for the driving side of profiles.

The proposed modification of geometry is based on application of a predesigned parabolic function of transmission errors and double crowning of pinion tooth surface. This enables to reduce the effect of gear misalignment.

The developed theory is illustrated with numerical examples.

2. Preliminary considerations and relations (pressure angles, base circles, lines of action, centrodes)

The asymmetry of profiles of discussed spur gears means that *different* pressure angles are applied for the driving and coast side profiles. Due to application of different pressure angles, the pinion and the gear are provided for two side profiles with base circles of different diameters. Fig. 1(a) and (b) show the pinion–gear base circles for the driving and coast sides, respectively. However, the *centrodes* (the operating pitch circles) are the same for both side profiles when the meshing of the pinion and the gear is considered. The centrodes are in tangency at point P that is the instantaneous center of rotation. The *line of action* for each side of profiles is the common tangent to the respective pair of base circles. The pressure angle is formed by the line of action and the tangent to the pitch circles.

Relation between pinion–gear tooth thicknesses: In case of a standard gear drive the tooth thicknesses s_p and s_g of the pinion and the gear (measured along the centrodes) are equal. However, the pinion and gear of an asymmetric gear drive are designed as nonstandard ones and parameters s_p and s_g are related as follows:

$$\lambda_t = \frac{s_p}{s_g}, \tag{1}$$

where λ_t is an assigned parameter

Due to rolling of centrodes, we have that

$$s_g = w_p, \tag{2}$$

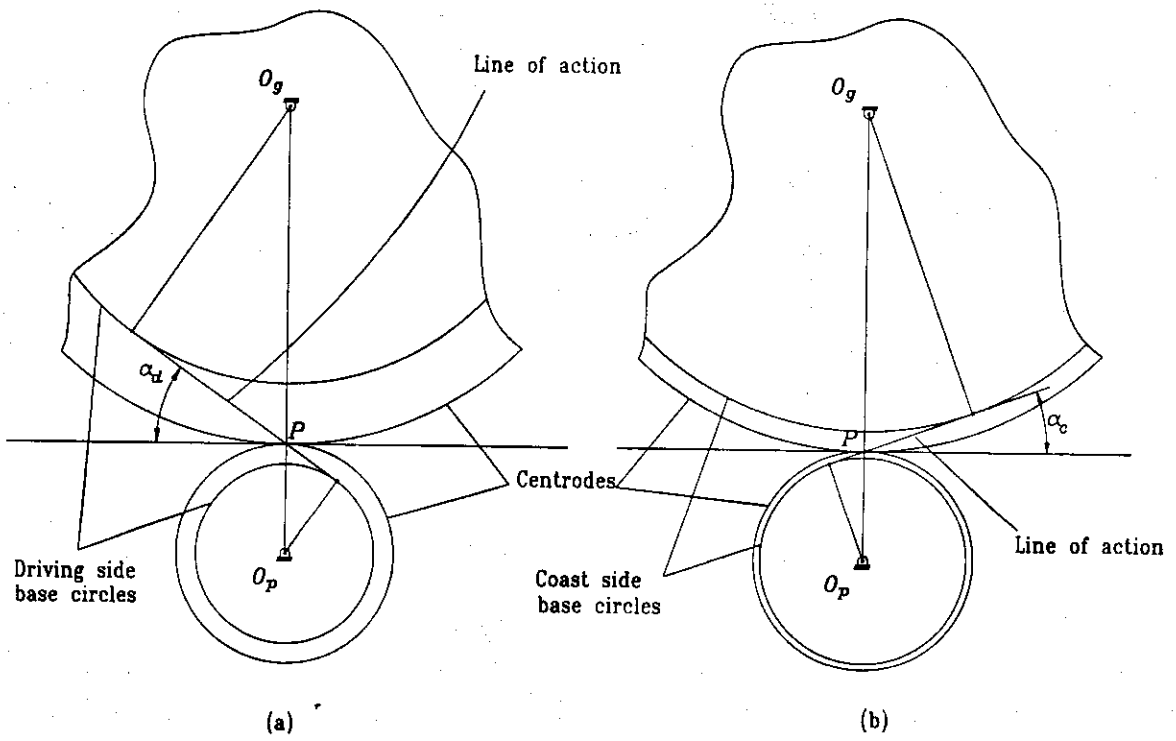

Fig. 1. Centrodes, lines of action and base circles in asymmetric gear drive.

$$s_p = w_g, \tag{3}$$

where w_k ($k = p, g$) is the width of space of the respective rack-cutter.

It is easy to be verified that

$$s_p + w_p = s_g + w_g = p = \frac{\pi}{P}, \tag{4}$$

where p and P are the circular and diametral pitches.

Then we obtain the following expressions for s_p and s_g

$$s_p = \frac{\lambda_t p}{1+\lambda_t} = \frac{\lambda_t \pi}{(1+\lambda_t)P}, \tag{5}$$

$$s_g = \frac{s_p}{\lambda_t} = \frac{p}{1+\lambda_t} = \frac{\pi}{(1+\lambda_t)P}. \tag{6}$$

Radii of base circles: The radius of the base circle and the radius of the centrode (operating pitch circle) are related by the equation

$$r_{bi} = r_p \cos \alpha_i = \frac{N}{2P} \cos \alpha_i, \quad (i = d, c), \tag{7}$$

where r_p is the radius of the respective centrode (of the pinion or the gear), N the respective number of teeth (of the pinion or the gear), P the diametral pitch and α_i the pressure angle.

Henceforth we will consider four base circles: two for the driving and coast sides of the pinion and two for the respective sides of the gear. There are two values α_d and α_c of the pressure angles, for the driving and coast sides, and α_d, (respectively, α_c) is the same for the pinion and the gear. The pairs of base circles of the pinion (respectively, of the gear) have a common center.

3. Analytical presentation of involute profiles

Drawings of Fig. 2 represent involute profiles of an asymmetric tooth. The drawings with specified designations can be referred to the pinion or to the gear.

We consider as given the following input: (i) $\widehat{DC} = s_p$, the tooth thickness on the pitch circle, (ii) radius r_p of the operating pitch circle, (iii) pressure angles α_d and α_c of the driving and coast profiles, (iv) radii of respective base circles r_{bd} and r_{bc} for the driving and coast sides. The goal is to represent analytically the tooth profiles.

Driving profile: The representation of the driving profile is based on following considerations (Fig. 2(a)):

Step 1. Point D_0 of the involute profile belongs to the base circle r_{bd} and its location with respect to point D is determined by the angle

$$\mathrm{inv}(\alpha_d) = \tan \alpha_d - \alpha_d. \tag{8}$$

Step 2. We represent the involute profile in coordinate system $S_d(x_d, y_d)$ which axis x_d is drawn from O to D_0. Instantaneous point M_d of the profile is identified by variable parameter ϕ_d. The equations of the profile are represented as follows [9]

$$\begin{aligned} x_d(\phi_d) &= r_{bd}(\cos \phi_d + \phi_d \sin \phi_d), \\ y_d(\phi_d) &= r_{bd}(\sin \phi_d - \phi_d \cos \phi_d). \end{aligned} \tag{9}$$

Coast profile: We represent the coast profile C_0–C–B in coordinate system S_c (Fig. 2(b)) by equations similar to Eq. (9)

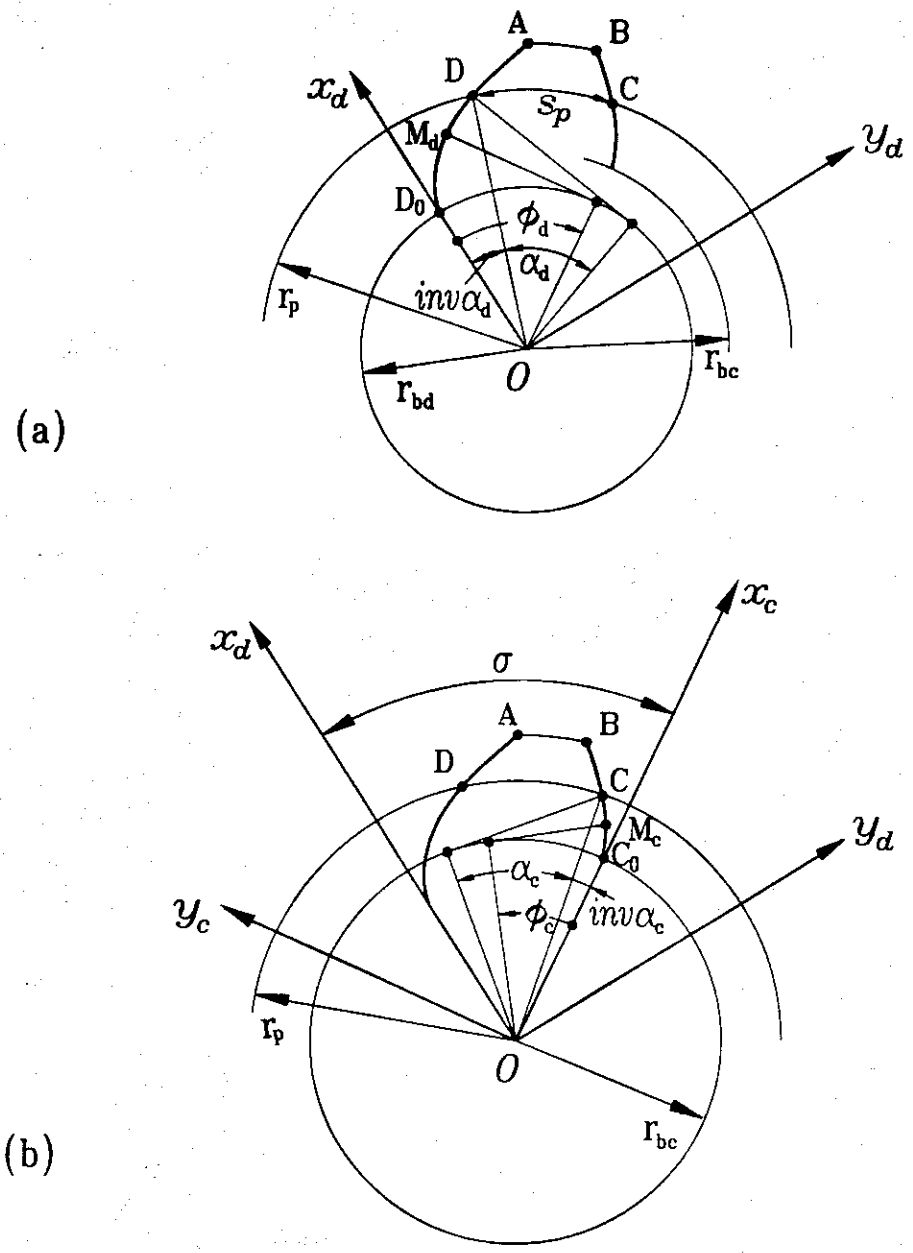

Fig. 2. Representation of driving profile (a), and coast profile (b).

$$x_c(\phi_c) = r_{bc}(\cos\ \phi_c + \phi_c \sin\ \phi_c),$$
$$y_c(\phi_c) = r_{bc}(\sin\ \phi_c - \phi_c \cos\ \phi_c). \tag{10}$$

The variable parameter ϕ_c determines current point M_c of coast profile. Axes x_d and x_c form angle σ that is determined by the following equation

$$\sigma = \mathrm{inv}(\alpha_d) + \frac{s_p}{r_p} + \mathrm{inv}(\alpha_c). \tag{11}$$

where $s_p = \widehat{DC}$ (Fig. 2(a)).

Addendum tooth thickness: Circular arc $\widehat{AB} = s_a$ represents the tooth thickness on the addendum circle of radius r_a (Fig. 3). We may determine s_a by using the following procedure of derivations:

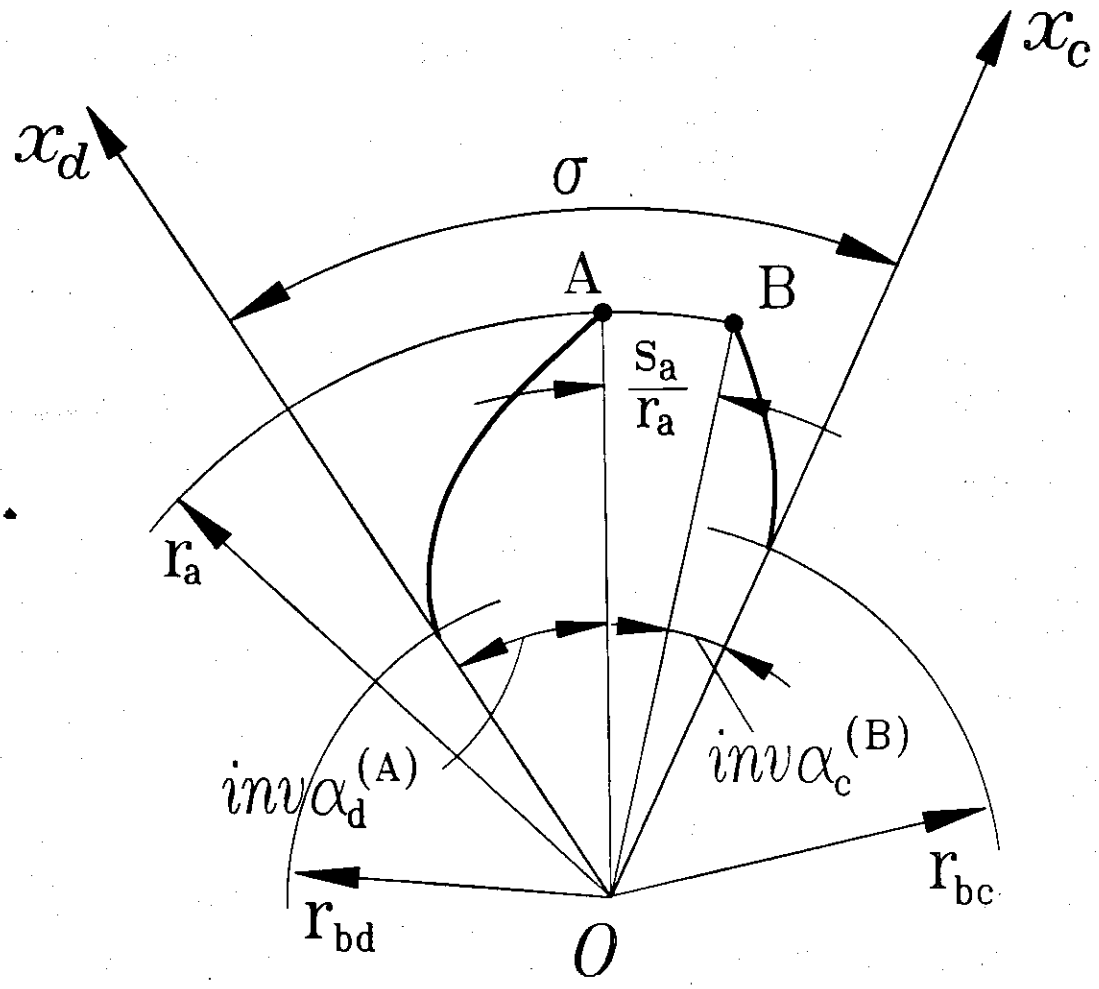

Fig. 3. For determination of addendum tooth thickness.

Step 1. Considering radius r_a as given, we obtain

$$\left(x_d^{(A)}\right)^2 + \left(y_d^{(A)}\right)^2 = r_a^2. \tag{12}$$

We designate by $\phi_d^{(A)}$ the variable parameter ϕ_d for point A of the driving profile (Fig. 2). Using Eqs. (9) and (12), we obtain

$$\phi_d^{(A)} = \sqrt{\left(\frac{r_a}{r_{bd}}\right)^2 - 1}. \tag{13}$$

Step 2. Taking into account that

$$\text{inv}(\alpha_d^{(A)}) = \tan\ \alpha_d^{(A)} - \alpha_d^{(A)}, \quad \tan\ \alpha_d^{(A)} = \phi_d^{(A)}.$$

we obtain that

$$\text{inv}(\alpha_d^{(A)}) = \phi_d^{(A)} - \arctan\ \phi_d^{(A)}. \tag{14}$$

Step 3. Similar derivations applied for the coast side yield that

$$\phi_c^{(B)} = \sqrt{\left(\frac{r_a}{r_{bc}}\right)^2 - 1},$$
$$\text{inv}(\alpha_c^{(B)}) = \phi_c^{(B)} - \arctan \phi_c^{(B)}. \tag{15}$$

Step 4. Drawings of Fig. 3 yield

$$s_a = r_a\left(\sigma - \mathrm{inv}(\alpha_d^{(A)}) - \mathrm{inv}(\alpha_c^{(B)})\right). \tag{16}$$

Here: parameter σ can be determined by using Eq. (11), $\mathrm{inv}(\alpha_d^{(A)})$ by using Eqs. (13) and (14), and $\mathrm{inv}(\alpha_c^{(B)})$ by using Eq. (15).

Step 5. The derived equations enable to obtain radius r_a for a pointing tooth taking in Eq. (16) that $s_a = 0$.

4. Design parameters of rack-cutter

Generation of conventional spur gears by a hob is based on the idea of meshing of spur gears with an imaginary rack-cutter. It is known from the theory of involute gearing, that the generation of a spur gear with the given radius of the base circle may be accomplished by a rack-cutter with a profile angle that differs from the pressure angle of the spur gear drive. The decrease of the profile angles α_d^* and α_c^* of the rack-cutter in comparison with the pressure angles α_d and α_c applied for the spur gear drive, enables to increase the radius of the rack-cutter fillet, obtain a more favorable fillet shape for the generated gears and reduce the bending stresses.

Determination of design parameters of the rack-cutter is based on the following procedure of derivations:

Step 1. The change of the profile angle of the rack-cutter will affect the radii of the centrodes of the pinion and consequently the gear being in mesh with the rack-cutter. Thus we have

$$r_p \cos \alpha_j = r_p^* \cos \alpha_j^* = r_{bj}, \quad (j = d, c), \tag{17}$$

where r_p and r_p^* are the radii of centrodes of the pinion being in mesh with the gear and the rack-cutter, respectively.

Similar equations can be derived for the gear of the drive.

Eq. (17) yield

$$\cos \alpha_c^* = \frac{\cos \alpha_c}{\cos \alpha_d} \cos \alpha_d^*. \tag{18}$$

Eq. (18) represents the relation between the profile angles α_c^* and α_d^* of the rack-cutter. One parameter of the couple of parameters (α_c^*, α_d^*) can be chosen and the other obtained from Eq. (18).

Step 2. The distance measured along the common normal to the driving or coast side profiles of the pinion (or the gear) must be the same as the distance measured between the respective profiles of the rack-cutter. Using this consideration, we obtain that the diametral pitch of the rack-cutter and spur gear drive are related as follows

$$P^* = P\frac{\cos \alpha_d^*}{\cos \alpha_d} = P\frac{\cos \alpha_c^*}{\cos \alpha_c}. \tag{19}$$

Step 3. We designate by s_p^* the tooth thickness of the pinion determined from the conditions of meshing of the pinion with the rack-cutter; s_p^* is measured on the centrode of the pinion being in mesh with the rack-cutter.

Drawings of Fig. 4 yield

$$s_p^* = r_p \frac{\cos \alpha_d}{\cos \alpha_d^*}\left(\frac{s_p}{r_p} + \mathrm{inv}(\alpha_d) - \mathrm{inv}(\alpha_d^*) + \mathrm{inv}(\alpha_c) - \mathrm{inv}(\alpha_c^*)\right). \tag{20}$$

Similarly we can determine the tooth thickness of the gear on its centrode determined from meshing of the gear with the rack-cutter.

The width of the space of the rack-cutter on the respective centrode is equal to the tooth thickness of the pinion (respectively, the gear) measured on the mentioned centrode.

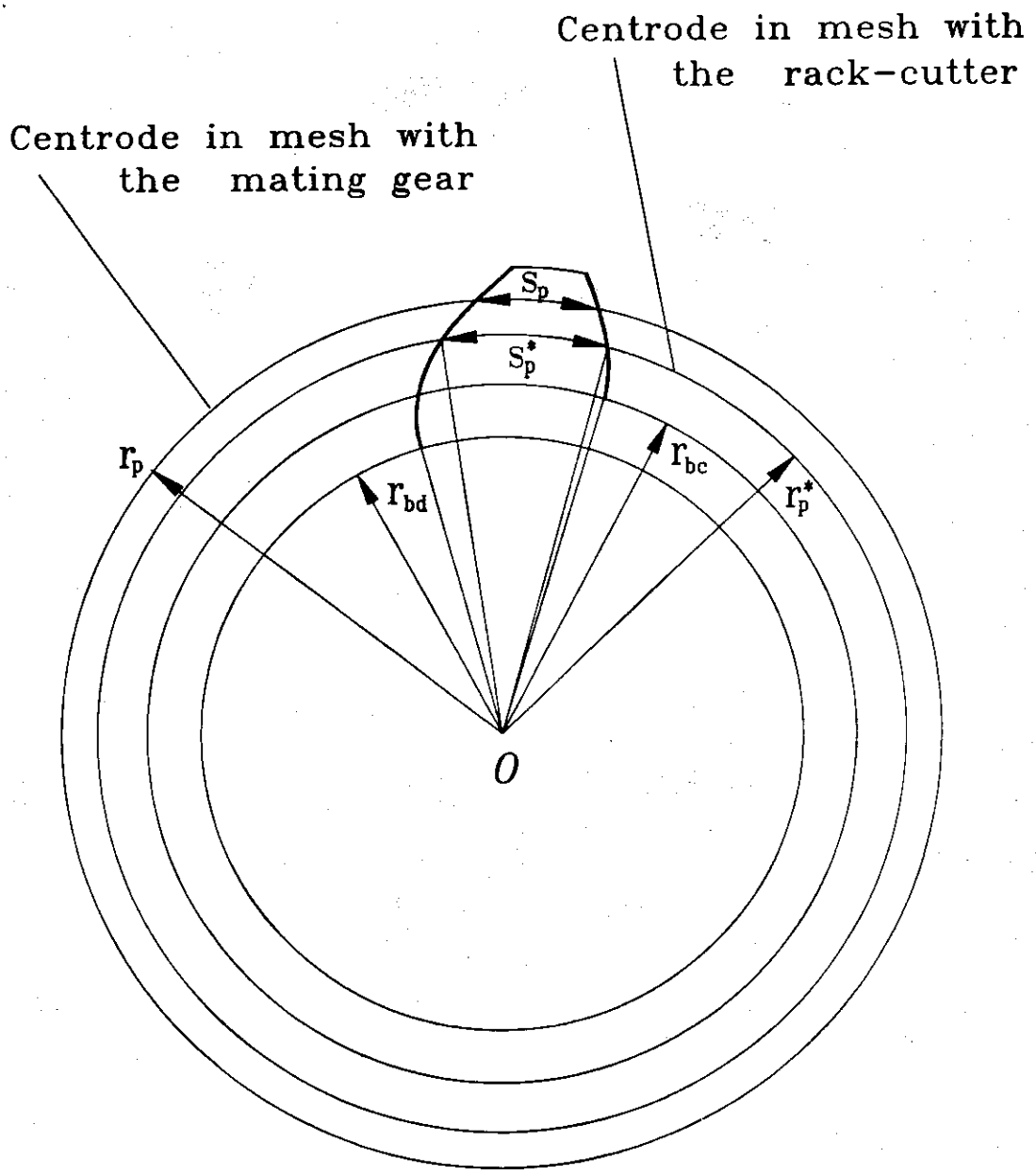

Fig. 4. For derivation of tooth thickness on centrodes in meshing with the rack-cutter and mating gear.

Step 4. Determination of radius ρ of the rack-cutter fillet (Fig. 6) is based on the following considerations:

(i) The working part of line of action of meshing pinion and gear is segment KL (Fig. 5) where K and L are the points of intersection of the line of action by the addendum circles of the pinion and the gear, respectively. Knowing the location of points K and L on both lines of action (for both side profiles) and considering the meshing of the rack-cutter with the pinion and the gear, we can determine such a point on the profile of the rack-cutter (designated as M in Fig. 6) that will provide a sufficient tooth length of the involute profile of the pinion and the gear.

It is necessary for this purpose to consider the meshing of the rack-cutter with both. the pinion and the gear, for both tooth sides: the driving and the coast sides. Usually, it is sufficient to consider the meshing of the rack-cutter and the driving side profile of the pinion.

(ii) Fig. 6 shows the middle line m–m of the rack-cutter, the centrode a–a of the rack-cutter being in mesh with the pinion. The extended profiles of the rack-cutter tooth form triangle ABD, where $\overline{AB} = \pi/P^* - s_p^*$ and the profile angles α_d^* and α_c^* are considered as known. The location of point M on the rack-cutter

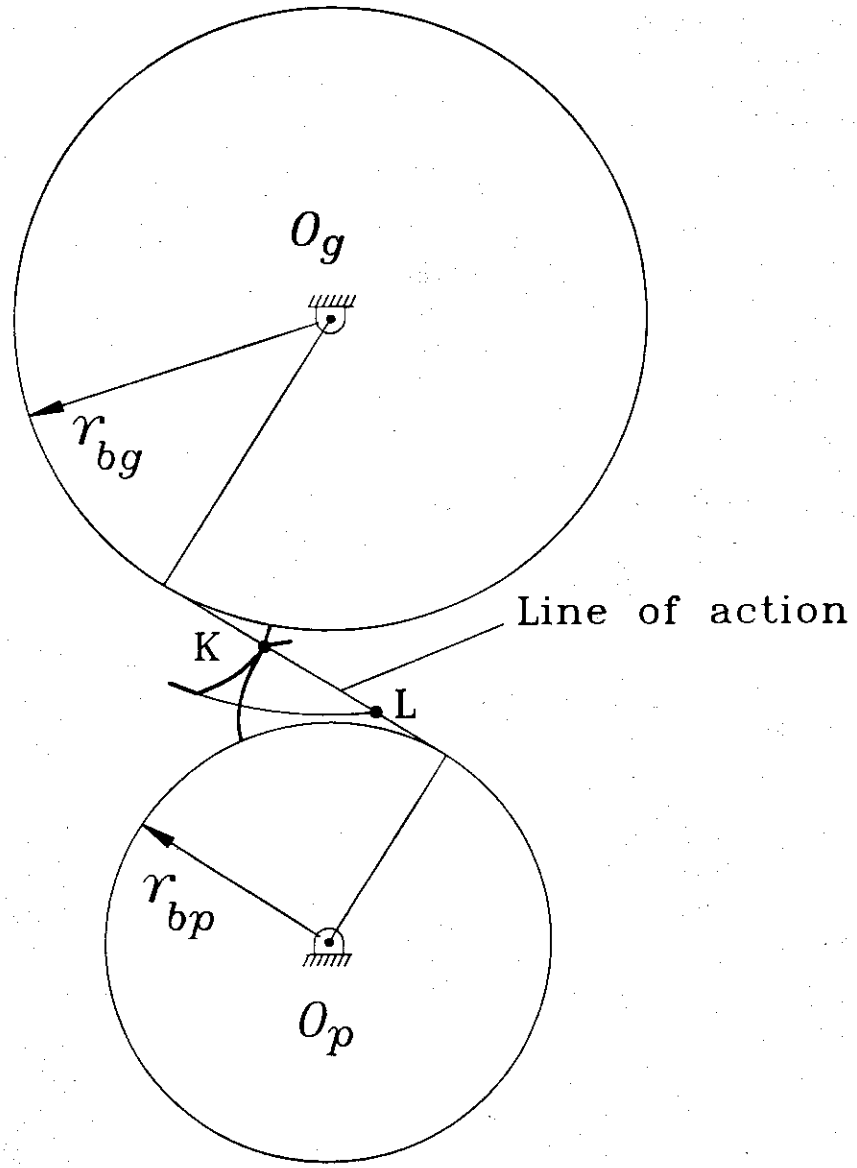

Fig. 5. Representation of working part KL of line of action.

profile is designated as $l_d = |\overline{BM}|$. It is easy to be verified that center C of the circular arc of the fillet belongs to the bisector of angle $\widehat{ADB}$. Drawings of Fig. 6 yield the following equation for determination of radius ρ of the rack-cutter fillet.

$$\rho = \frac{\overline{AB}\cos\alpha_c^* - l_d \sin\left(\alpha_d^* + \alpha_c^*\right)}{2\cos^2\left(\alpha_d^* + \alpha_c^*/2\right)}. \tag{21}$$

Parameter l_d in Eq. (21) is determined by considering the conditions of meshing of the rack-cutter with the generated pinion and gear. Point M of the rack-cutter generates the respective point of the involute profile of the pinion and the gear that might be the limiting point of the addendum profile.

5. Modification of tooth geometry: basic principles

Double crowning of pinion: The purposes of modification of tooth geometry are: (i) reduction of noise, and (ii) localization of bearing contact. Both goals are achieved by double- crowning of the pinion tooth surface, in profile and longitudinal directions. Profile crowning enables to reduce the magnitude of

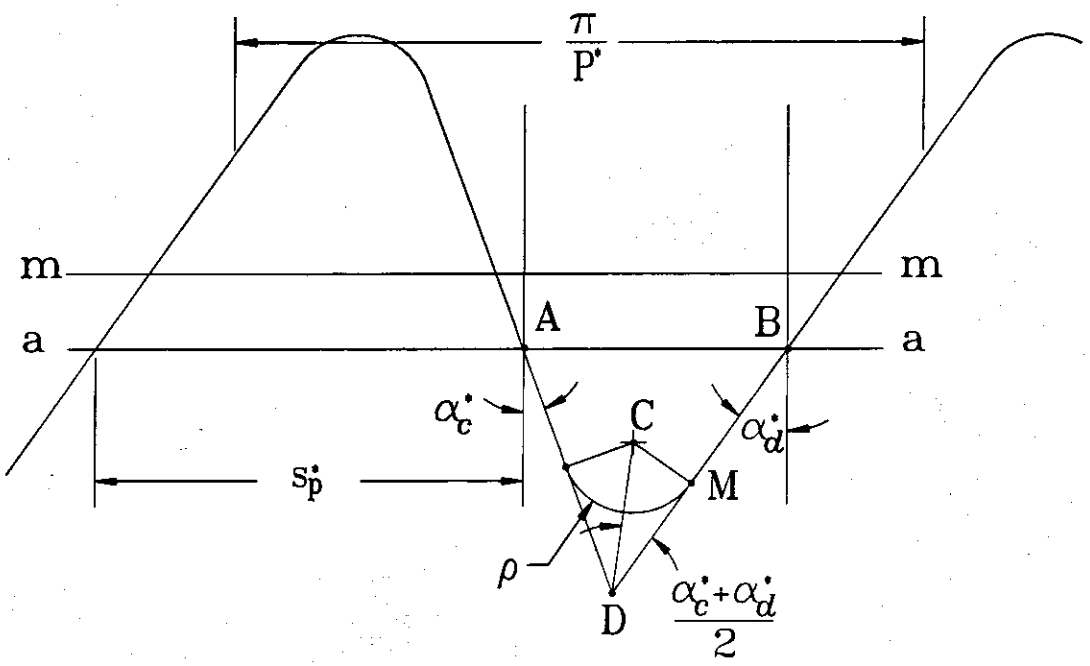

Fig. 6. For determination of radius ρ of the rack-cutter fillet.

transmission errors and obtain a favorable shape of such errors caused by misalignment; transmission errors are caused by gear misalignment. Longitudinal crowning of the pinion enables to substitute instantaneous line contact of pinion–gear tooth surfaces by instantaneous point contact. Then, the bearing contact becomes localized, located in the middle of gear tooth surfaces, and edge contact (caused by misalignment) can be avoided.

We remind that transmission errors of a misaligned gear drive are the source of vibration and noise. Edge contact is the result of the shift of bearing contact due to misalignment of pinion- gear tooth surfaces being in instantaneous line contact.

Point contact of tooth surfaces is spread under the load on an elliptical area. Therefore, the real bearing contact of a loaded gear drive is formed as a set of instantaneous contact ellipses.

The concept of pinion profile crowning is based on application of two imaginary mismatched rack-cutters which cross-section profiles are represented in Fig. 7. The profile of the gear rack-cutter is a straight line and the pinion rack-cutter has a parabolic profile. Due to the mismatch of profiles of mating rack-cutters, by designating a proper parabola coefficient for the pinion parabolic rack-cutter, it becomes possible to control the transmission errors of a misaligned spur gear drive.

The concept of longitudinal crowning is based on variation of the plunging tool in the process of pinion generation. The plunge of the tool that is a grinding disk (Fig. 8) provides longitudinal crowning of pinion tooth surface.

Pinion profile crowning: Fig. 7 shows the mismatched profiles of the gear and rack- cutter cross-section profiles that are a straight line and a parabolic curve, respectively. The profiles mentioned above are in tangency at points Q_d on the driving side and Q_c on the coast side. The normals to the profiles at points Q_d and Q_c pass through point P that lies on the center distance of the gear drive.

The surfaces of the rack-cutters are a plane and a parabolic cylinder. It is assumed that the gear and pinion rack-cutters generate the gear and pinion separately. The pinion and gear tooth surfaces (generated by rack-cutters mentioned above) are in line contact in an aligned gear drive. The instantaneous lines of tangency of pinion and gear tooth surfaces are parallel to their axes of rotation (in an aligned gear drive). However, the transformation of rotation by the gear drive is not performed with a constant gear ratio $m_{12} = \omega^{(1)}/\omega^{(2)}$ since the pinion rack-cutter profile is mismatched with respect to the gear rack-cutter.

Usually, errors of alignment $\Delta\phi_2(\phi_1)$ of a gear drive cause a piecewise transformation function $\phi_2(\phi_1)$. The function of transmission errors $\Delta\phi_2(\phi_1)$ is determined as

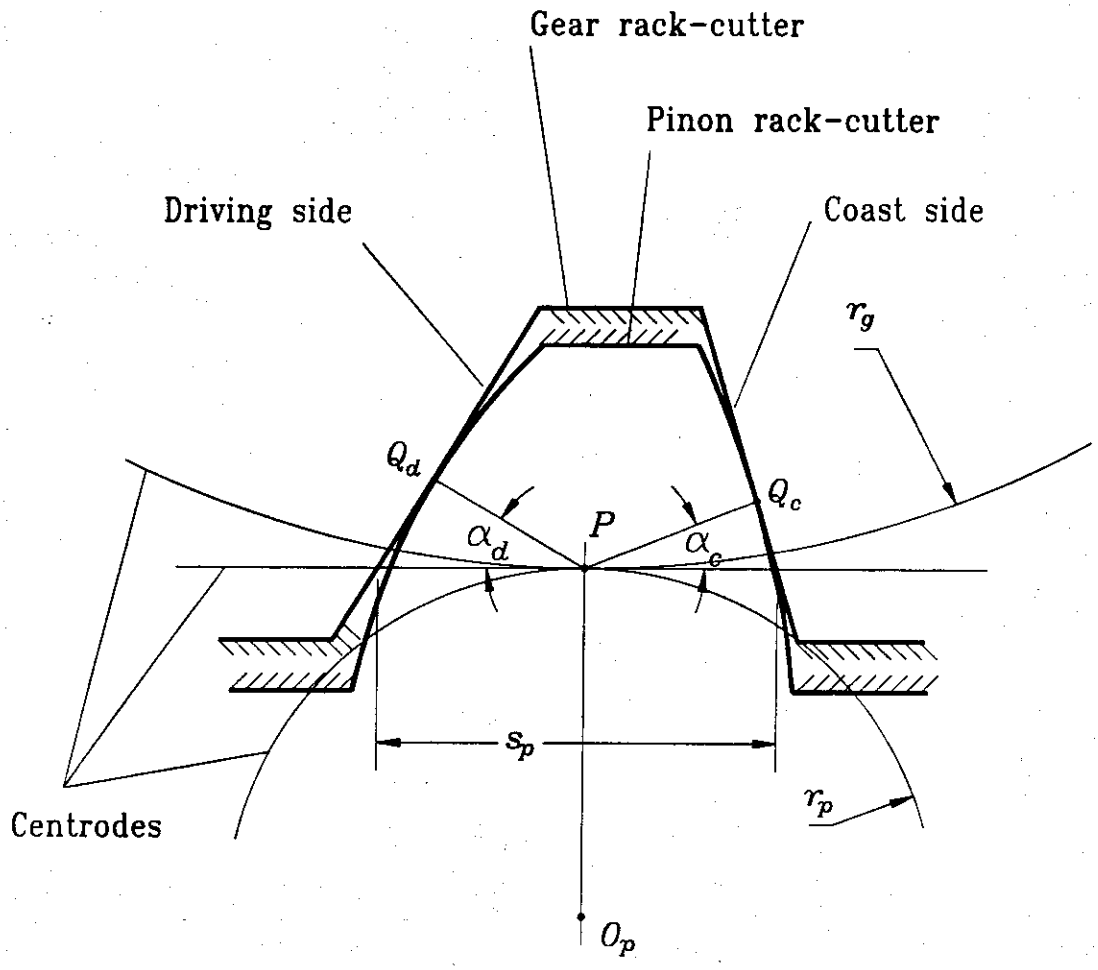

Fig. 7. Imaginary rack-cutters applied for generation of the gear and pinion.

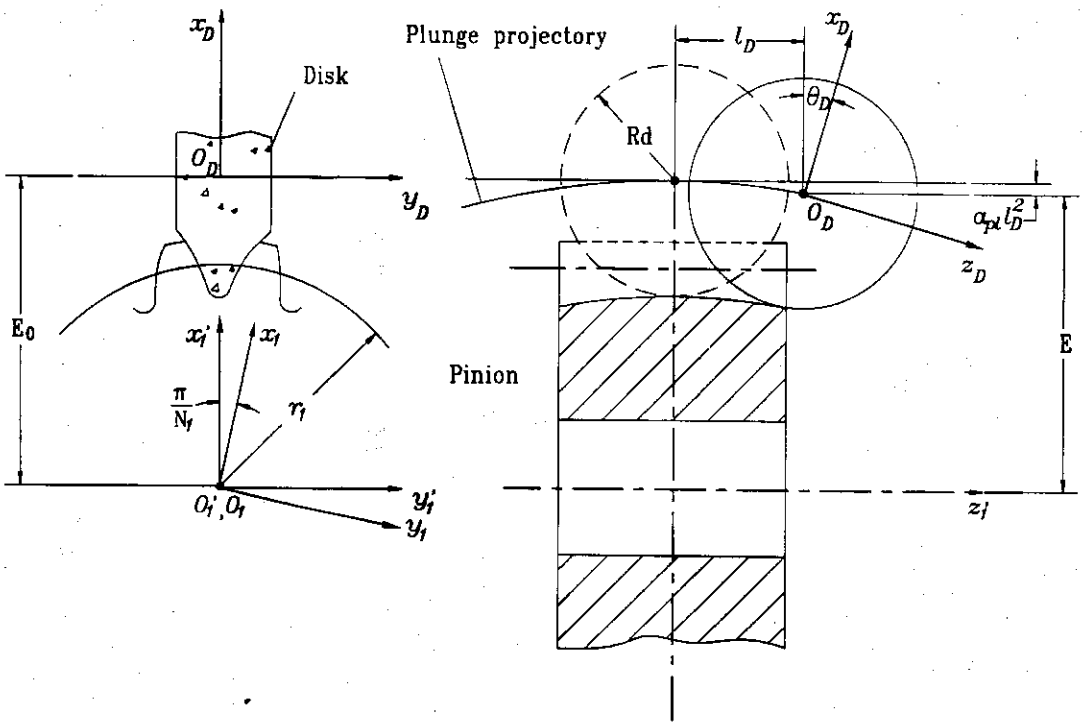

Fig. 8. Grinding disk for pinion longitudinal crowning.

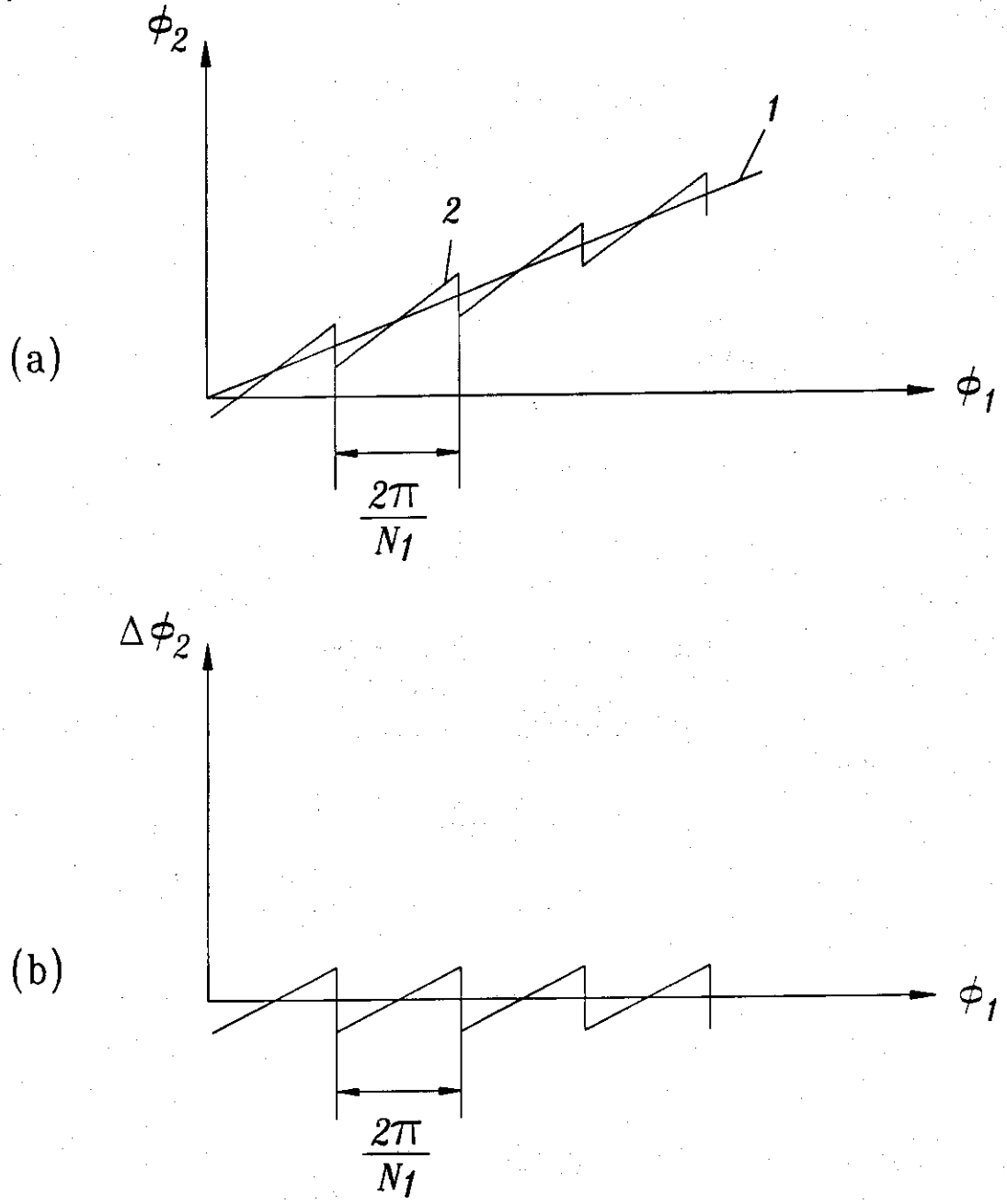

Fig. 9. Transmission function of misaligned geare drive (a); function of transmission errors (b).

$$\Delta\phi_2(\phi_1) = \phi_2(\phi_1) - \frac{N_1}{N_2}\phi_1, \tag{22}$$

where ϕ_1 and ϕ_2 are the angles of rotation of the pinion and the gear, N_1 and N_2 the pinion and gear tooth numbers. It is proven in [9] that function $\phi_2(\phi_1)$ of transmission errors is a discontinuous almost linear function (Fig. 9), and the transfer of meshing between the neighboring teeth is accompanied with noise and vibration.

The purpose of application of a parabolic profile of the pinion rack-cutter is to provide a *parabolic* function of transmission errors represented as

$$\Delta\phi_2(\phi_1) = -a\phi_1^2. \tag{23}$$

Such a function is able to absorb linear functions of transmission errors caused by errors of alignment [9,10] and therefore reduce vibration and noise of the gear drive. In addition, due to pinion profile crowning, the

conditions of transfer of meshing between the neighboring teeth are improved as well. This is achieved by the decrease of elastic deformation of teeth at the transfer of meshing.

Longitudinal crowning: It was mentioned above that pinion profile crowning does not enable to substitute the instantaneous line contact of pinion–gear tooth surfaces by point contact. Point contact due to the tool plunging is achieved by the execution of the equation

$$E - E_0 = -a_{pl} l_D^2. \tag{24}$$

Here: E_0 and E are the initial and current center distance; l_D the displacement of the tool in direction parallel to pinion axis (measured from the middle of tooth length); a_{pl} the parabola coefficient in parabolic function (24).

The pinion tooth surface generated by the plunging disk is determined as the sequence of two enveloping processes.

The first enveloping process provides an intermediate pinion tooth surface $\Sigma_1^{(1)}$ as the envelope to the family of parabolic rack-cutter surfaces. The cross-section of $\Sigma_1^{(1)}$ is the axial profile of the disk surface Σ_D (see Appendix A).

The second enveloping process provides the final pinion tooth surface $\Sigma_1^{(2)}$ as the envelope to the family of surfaces generated by the plunging disk. It is important to recognize that $\Sigma_1^{(2)}$ is not a cylindrical surface as the tooth surface of a conventional spur gear.

Finally, we can state that the proposed gear drive formed by a double-crowning pinion tooth surface and a conventional spur involute tooth surface for the gear have the following features: (i) the tooth surfaces are in point contact at every instant, and (ii) their meshing is accompanied with a predesigned parabolic function of transmission errors (see Fig. 10 and Section 7).

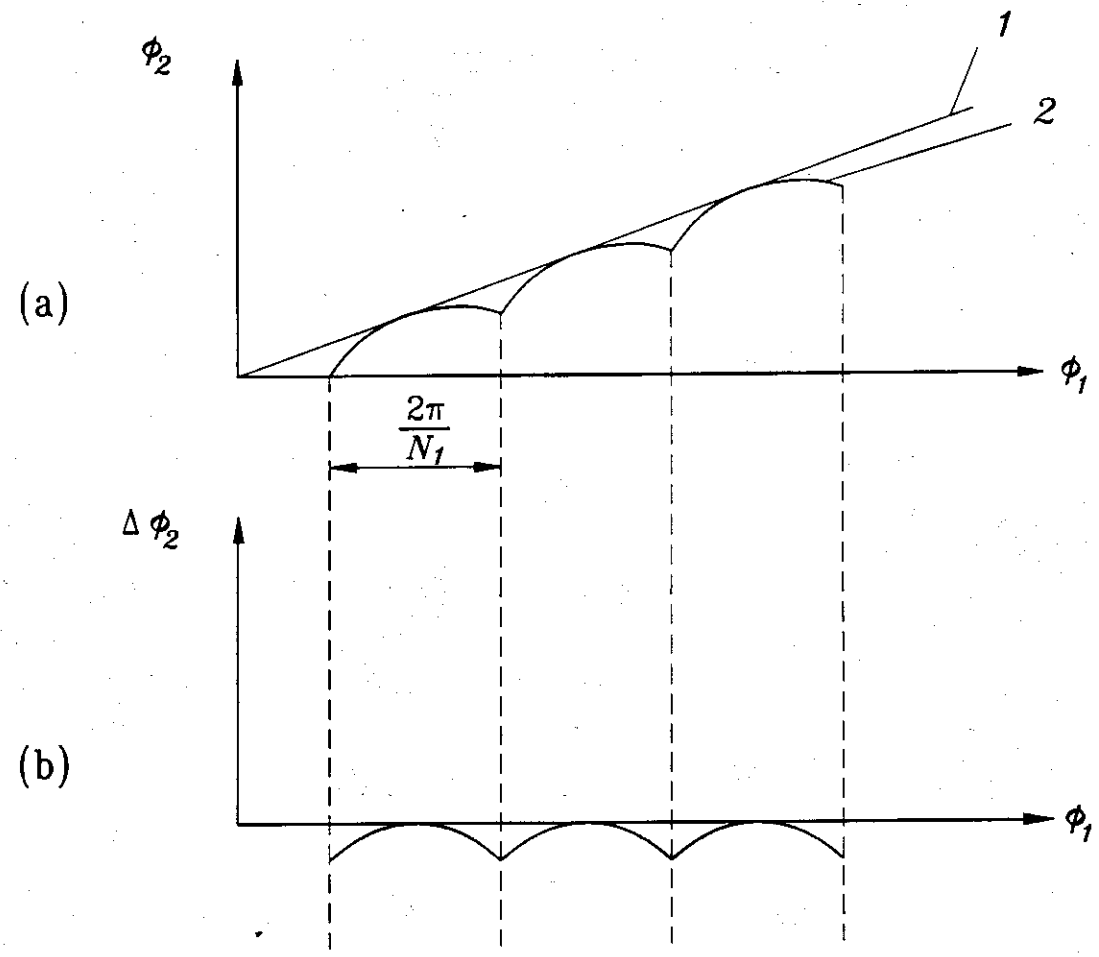

Fig. 10. Transmission function (a), and parabolic function of transmission errors (b).

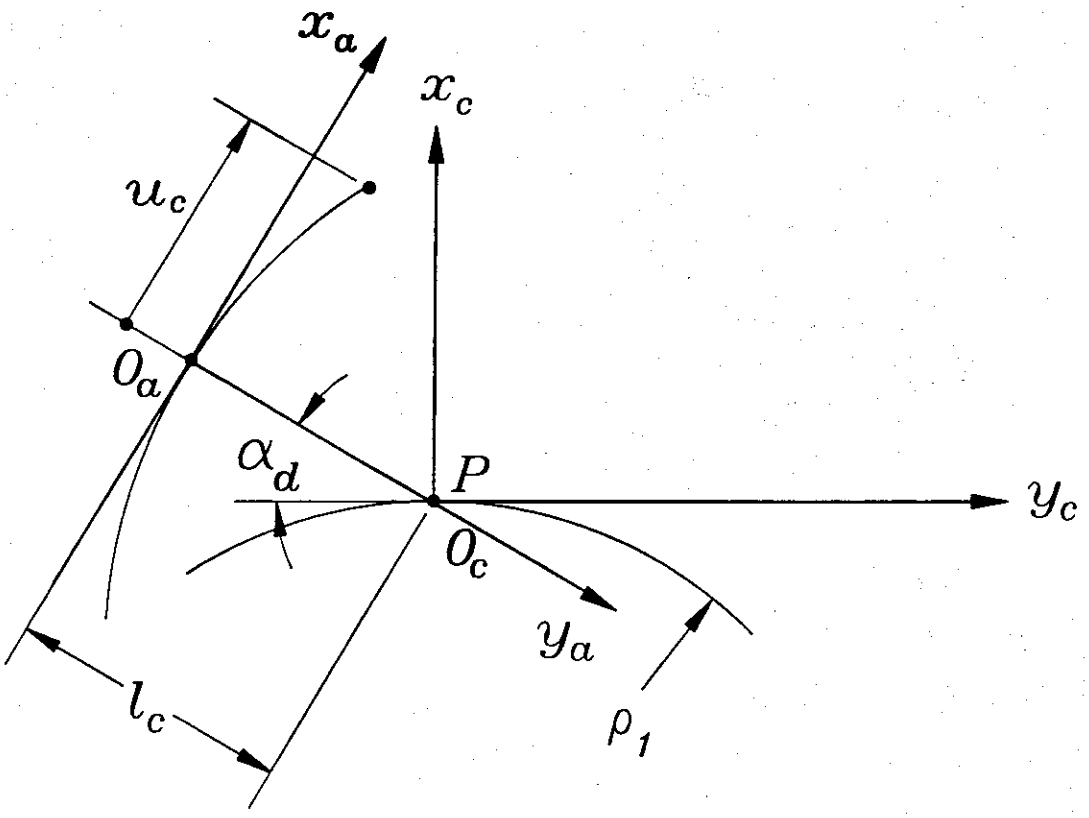

Fig. 11. Pinion parabolic rack-cutter.

6. Equations of pinion parabolic rack-cutter

We limit the derivations to the case of pinion parabolic rack-cutter for the driving side. The pinion rack-cutter surface Σ_c is a parabolic cylinder and is represented in the auxiliary coordinate system S_a (Fig. 11) as

$$\mathbf{r}_a(u_c, \theta_c) = \begin{bmatrix} u_c \\ a_c u_c^2 \\ \theta_c \\ 1 \end{bmatrix}. \tag{25}$$

The normal to the rack-cutter surface Σ_c is represented as

$$\mathbf{N}_a(u_c) = \mathbf{k}_a \times \frac{\partial \mathbf{r}_a}{\partial u_c} = \begin{bmatrix} -2a_c u_c \\ 1 \\ 0 \end{bmatrix}. \tag{26}$$

Origin O_a of S_a coincides with point Q_d of tangency of gear and pinion rack-cutters (Fig. 7).

The rack-cutter surface Σ_c and its normal are represented in coordinate system S_c by the matrix equations

$$\mathbf{r}_c(u_c, \theta_c) = \mathbf{M}_{ca}\mathbf{r}_a, \tag{27}$$

$$\mathbf{N}_c(u_c) = \mathbf{L}_{ca}\mathbf{N}_a. \tag{28}$$

7. Relation between parabola coefficients a_c, a and $\Delta\phi_{2\,\max}$

Coefficient a_c represents the parabola coefficient of the parabolic profile of pinion rack-cutter (see Eq. (25)). Coefficient a represents the parabola coefficient in the equation of the predesigned parabolic function of transmission errors determined as

$$\Delta\phi_2(\phi_1) = \phi_2(\phi_1) - \phi_1\frac{N_1}{N_2} = -a\phi_1^2. \tag{29}$$

The negative sign in Eq. (29) means that the gear must lag in comparison with the pinion in the process of transformation of rotation.

Our goal is to determine the relations between coefficients a_c and a that enable to determine the predesigned parabolic function of transmission errors locally, considering as given the derivative of function $\Delta\phi_2(\phi_1)$ at $\phi_1 = 0$. The other goal is to represent parabola coefficients a_c and a considering as given $|\Delta\phi_{2\max}|$ for a cycle of meshing. The derivations are based on the following procedure:

Step 1. Eq. (29) yields that

$$|\Delta\phi_{2\max}| = a\left(\frac{\pi}{N_1}\right)^2, \tag{30}$$

where π/N_1 determines the cycle of meshing.

Considering that $|\Delta\phi_{2\max}|$ is given in arc sec., we obtain the following equation for the parabola coefficient a

$$a = \frac{|\Delta\phi_{2\max}|N_1^2}{\pi(180)(3600)}. \tag{31}$$

Step 2. We apply Eqs. (8.3.39) and (8.3.32) derived in [9] that relate: (i) the curvatures of the pinion and rack-cutter profiles, and (ii) the pinion and gear profiles. After transformations. we obtain the following relation between the curvature κ_d of the pinion rack-cutter profile and the derivative m_{21}'

$$F\left(\kappa_d, m_{21}'\right) = A[(\rho_1 + \rho_2)(1 - \kappa_d L_d) + \kappa_d\rho_1\rho_2 \sin\alpha_d] - B\rho_2 = 0. \tag{32}$$

Here:

$$A = (\rho_1 + \rho_2)\frac{N_1}{N_2}\sin\alpha_d + m_{21}'\rho_2\cos\alpha_d, \tag{33}$$

$$B = \rho_1 \sin\alpha_d\left(1 + \frac{N_1}{N_2}\right)^2(1 - \kappa_d L_d), \tag{34}$$

$$m_{21}' = \frac{\partial^2}{\partial\phi_1^2}[\phi_2(\phi_1)], \tag{35}$$

where $\phi_2(\phi_1)$ is the transmission function of the gear drive; ρ_1 and ρ_2 the radii of the pinion and gear centrodes being in mesh with the imaginary rack-cutters; $L_d = |\overline{Q_dP}|$ (Fig. 7).

Eqs. (35) and (29) yield that

$$m_{21}' = -2a. \tag{36}$$

Step 3. Using equation of curvature of a planar gearing in [9], we obtain the following expression for the curvature of the parabolic rack-cutter profile at point O_d in Fig. 11.

$$\kappa_d = 2a_c \tag{37}$$

Step 4. Eqs. (37), (36), (31) and (32) enable to obtain the coefficient a_c for the pinion parabolic rack-cutter considering as given $|\Delta\phi_{2\max}|$.

Numerical example 1. Parameters of the asymmetric gear drive are: $N_1 = 23$, $N_2 = 70$, $P = 8\frac{1}{in}$, $\alpha_d = 35°$, $\alpha_c = 20°$, $|\Delta\phi_{2\max}| = 5$ arc s.

Using the procedure discussed above, we obtain that $a = 0.0013$, and $a_{cd} = 0.0069$, $a_{cc} = 0.02235$ for the driving, and coast side profiles, respectively.

8. Simulation of meshing and contact

Simulation of meshing: The algorithm of meshing provides conditions of continuous tangency of tooth surfaces in an aligned and misaligned gear drives. The precondition of pinion-gear tooth surfaces to be in point contact is observed. The simulation of meshing of the analyzed gear drive is computerized and the output of the program are: (i) the paths of contact on pinion and gear tooth surfaces, and (ii) the transmission errors caused by misalignment.

The algorithm developed for simulation of meshing is based on the following considerations:

(1) We apply movable coordinate systems S_1 and S_2 (Fig. 12) that are rigidly connected to the pinion and the gear, and the fixed coordinate system S_f where the meshing of surfaces is considered. An auxiliary coordinate system S_q (Fig. 12) is applied for simulation of errors of alignment ΔE-the change of center distance and $\Delta\gamma$-the change of the shaft angle.

(2) We represent the conditions of continuous tangency of tooth surfaces by the following equations:

$$\begin{aligned} &\mathbf{r}_f^{(1)}(u_c, \theta_D, \phi_1) - \mathbf{r}_f^{(2)}(u_t, \theta_t, \phi_2) = \mathbf{0}, \\ &\mathbf{n}_f^{(1)}(u_c, \theta_D, \phi_1) - \mathbf{n}_f^{(2)}(u_t, \theta_t, \phi_2) = \mathbf{0}. \end{aligned} \tag{38}$$

Eq. (38) represent that surfaces Σ_1 and Σ_2 have a common point and have at this point a common normal. Vector Eq. (38) yield a system of only five independent scalar equations in six unknowns since $|\mathbf{n}_f^{(1)}| = |\mathbf{n}_f^{(2)}| = 1$. Thus we obtain

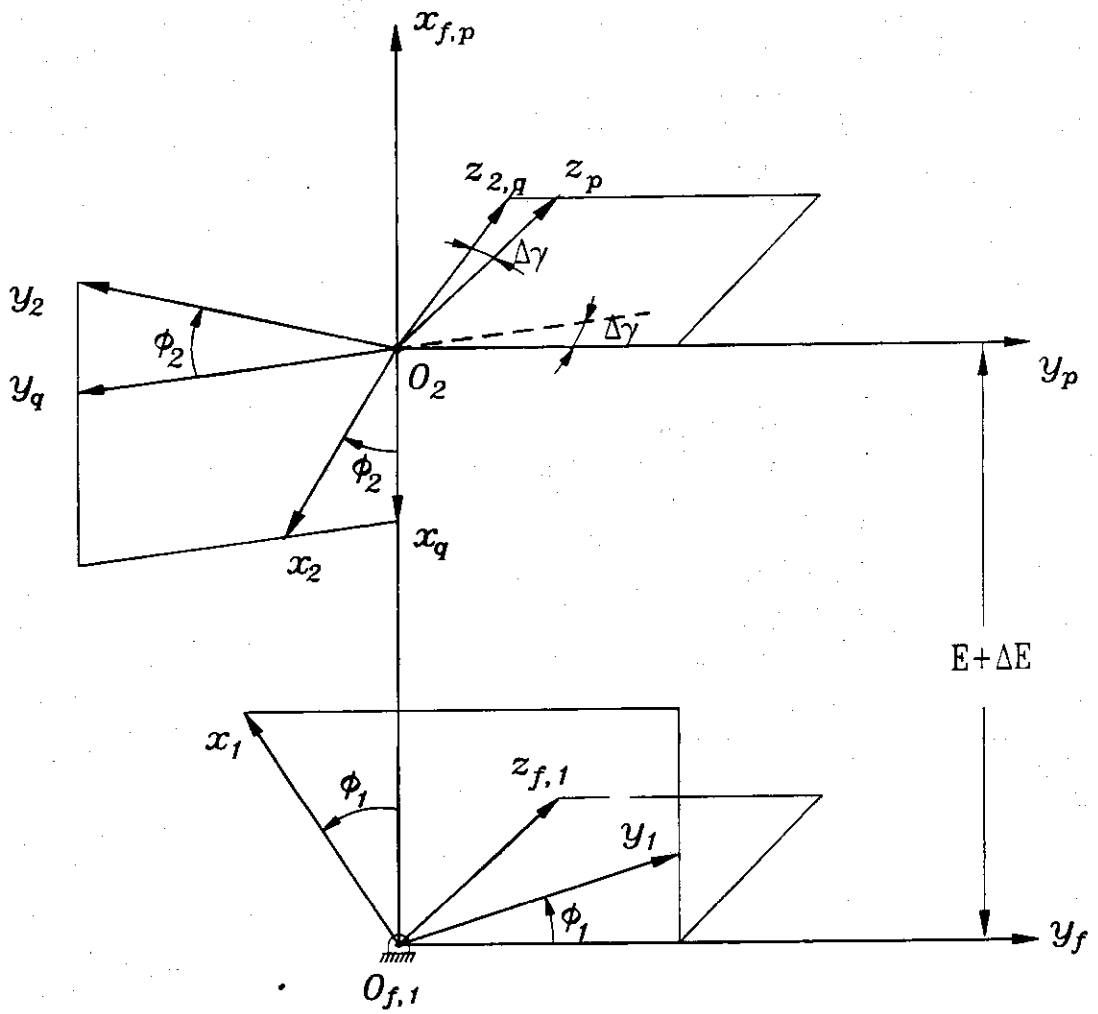

Fig. 12. Coordinate systems applied for TCA.

$$f_i(u_c, \theta_D, \phi_1, u_t, \theta_t, \phi_2) = 0, \quad f_i \in C'' \ (i = 1, \ldots, 5). \tag{39}$$

We consider now the solution of equation system (39) with the following preconditions:

(i) There is a set of parameters (obtained as the first guess) designated as

$$P = (u_c^0, \theta_D^0, \phi_1^0, u_t^0, \theta_t^0, \phi_2^0)$$

that satisfy Eq. (39)

(ii) One of the six parameters, say ϕ_1, is considered as the input one and the Jacobian of the system of equations differs at P from zero. Thus

$$\frac{D(f_1, f_2, f_3, f_4, f_5)}{D(u_c, \theta_D, u_t, \theta_t, \phi_2)} \neq 0. \tag{40}$$

(iii) It follows from the theorem of implicit function existence [10], that the system of Eq. (39) can be solved in the neighborhood of P by functions

$$\{u_c(\phi_1), \theta_D(\phi_1), u_t(\phi_1), \theta_t(\phi_1), \phi_2(\phi_1)\} \in C'. \tag{41}$$

Then, it becomes possible as shown in [9] to obtain the paths of contact on gear tooth surfaces, the transmission function $\phi_2(\phi_1)$, and the transmission errors $\Delta\phi_2(\phi_1)$.

The solution of the system of nonlinear Eq. (39) is an iterative process and is supported by application of the subroutine DNEQNF in IMSL library [7].

The results of computation by the developed computer program are illustrated by drawings of Figs. 13–17. Two cases of design are considered:

Case 1. Two rack-cutters with coinciding straight line profiles are considered, profile crowning is not provided, but longitudinal crowning of the pinion is provided by the plunging of the pinion grinding disk to obtain point contact of pinion–gear tooth surfaces.

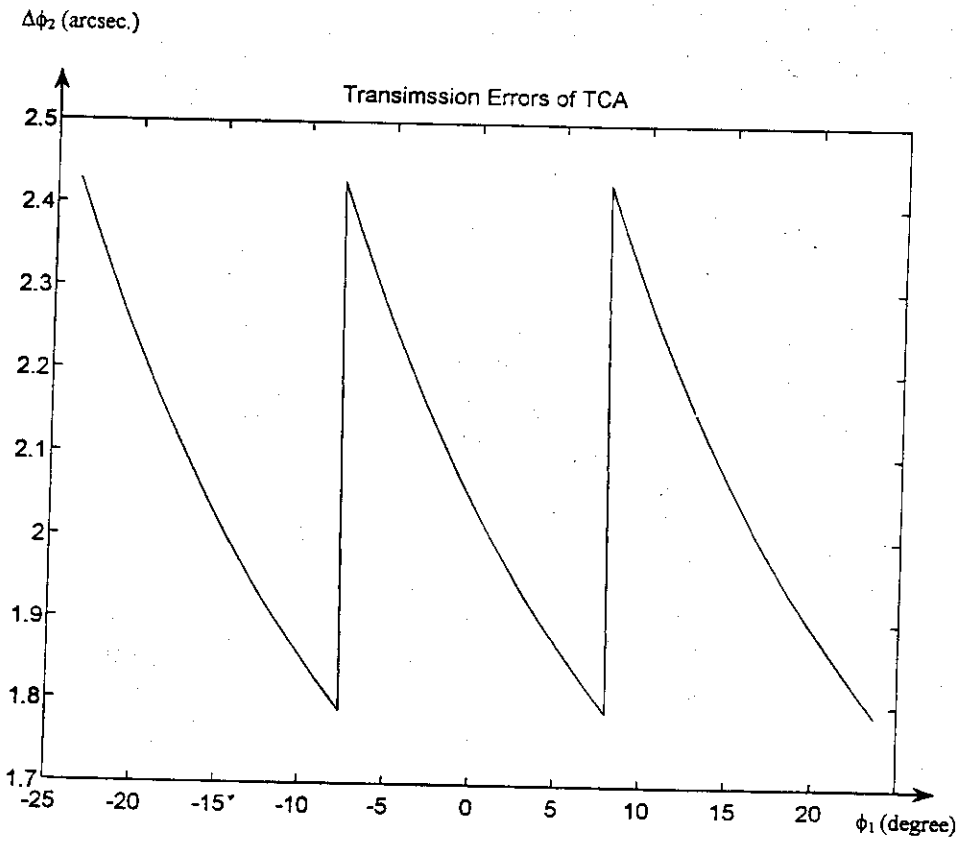

Fig. 13. Function of transmission errors $\Delta\phi_2(\phi_1)$ caused by $\Delta\gamma = 3$ arcmin; generation Case 1.

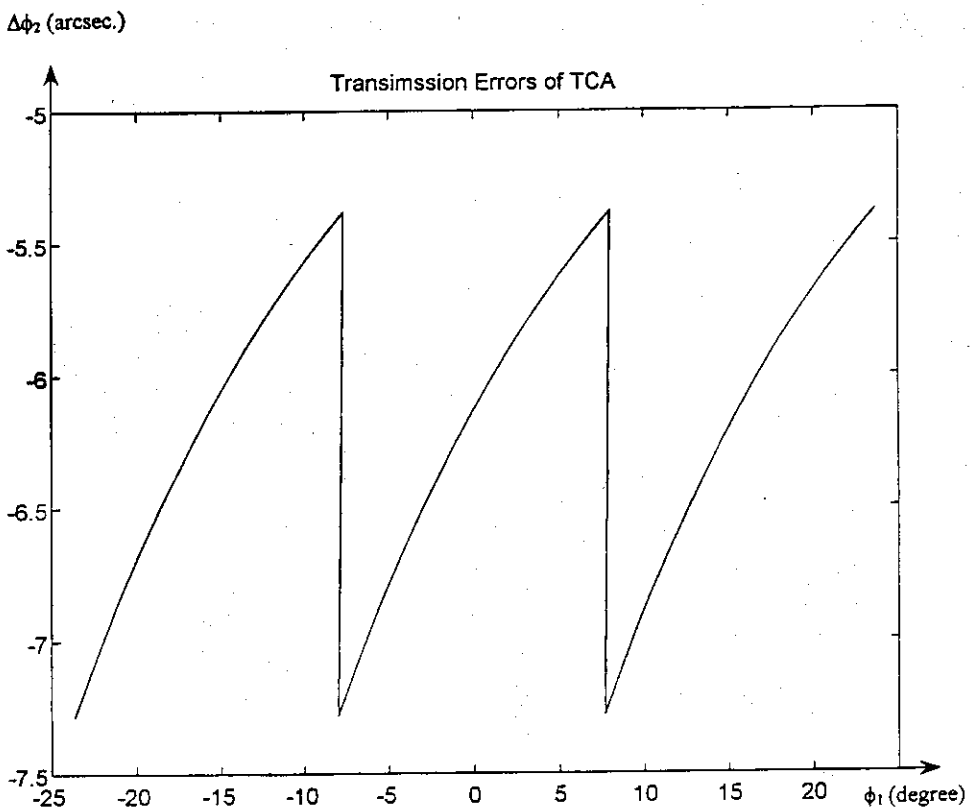

Fig. 14. Function of transmission errors $\Delta\phi_2(\phi_1)$ caused by $\Delta\lambda = 3$ arcmin; generation Case 1.

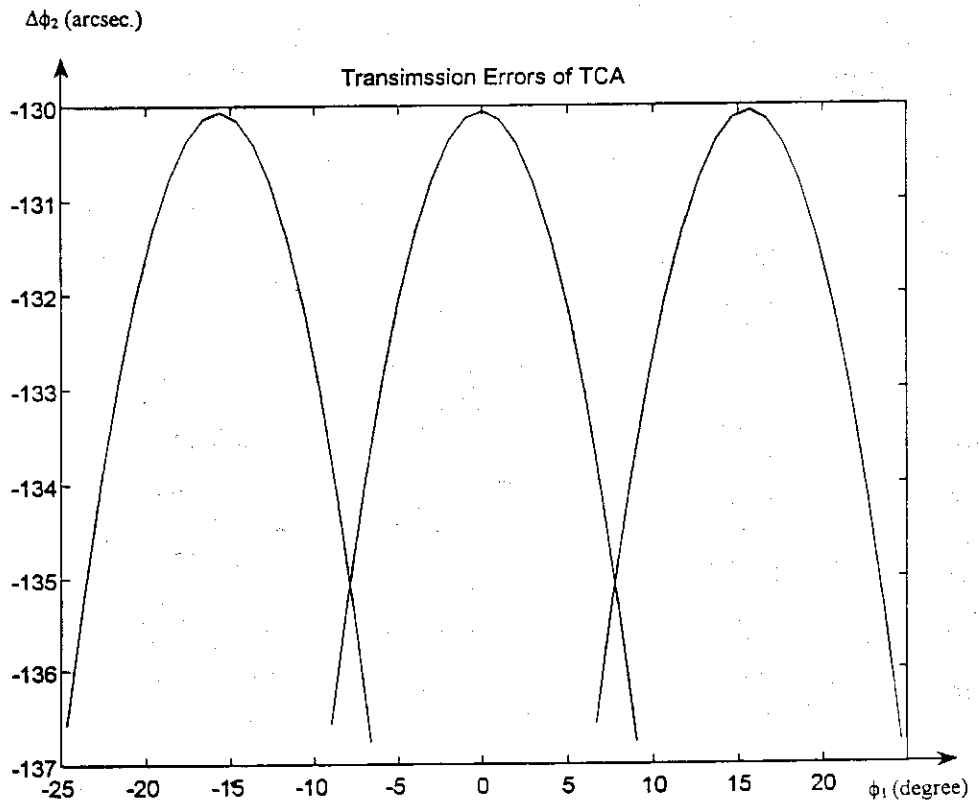

Fig. 15. Function of transmission errors $\Delta\phi_2(\phi_1)$ caused by $\Delta E = 0.1$ mm; generation Case 2.

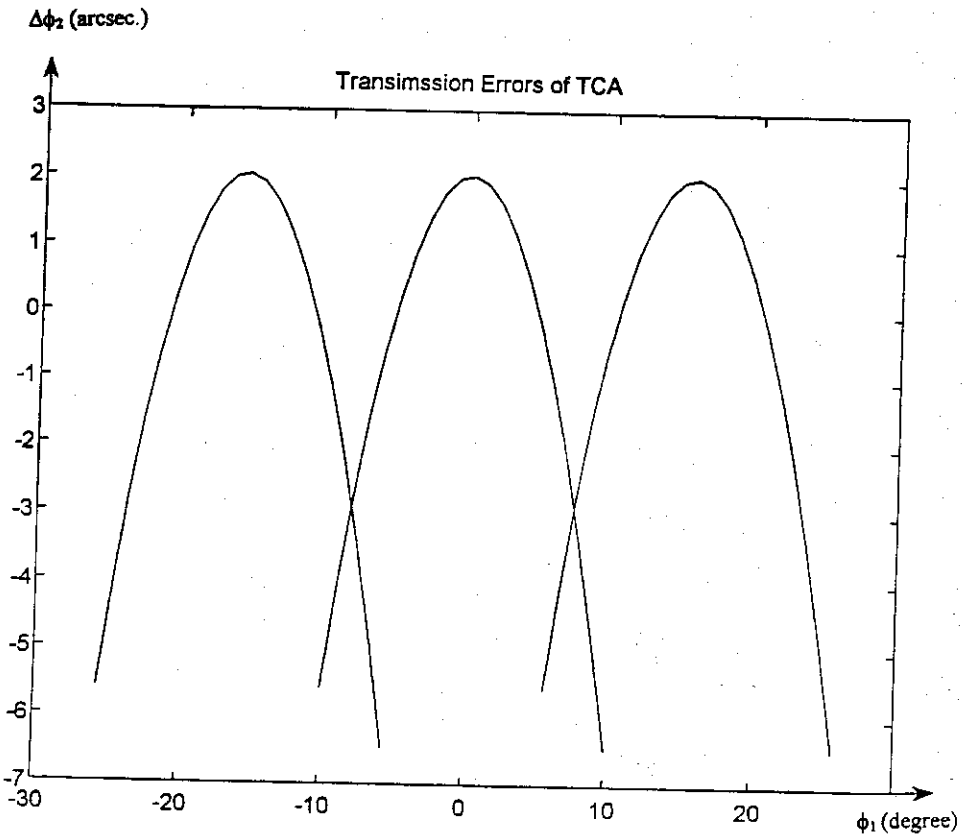

Fig. 16. Function of transmission errors $\Delta\phi_2(\phi_1)$ caused by $\Delta\tilde{\gamma}' = 3$ arcmin; generation Case 2.

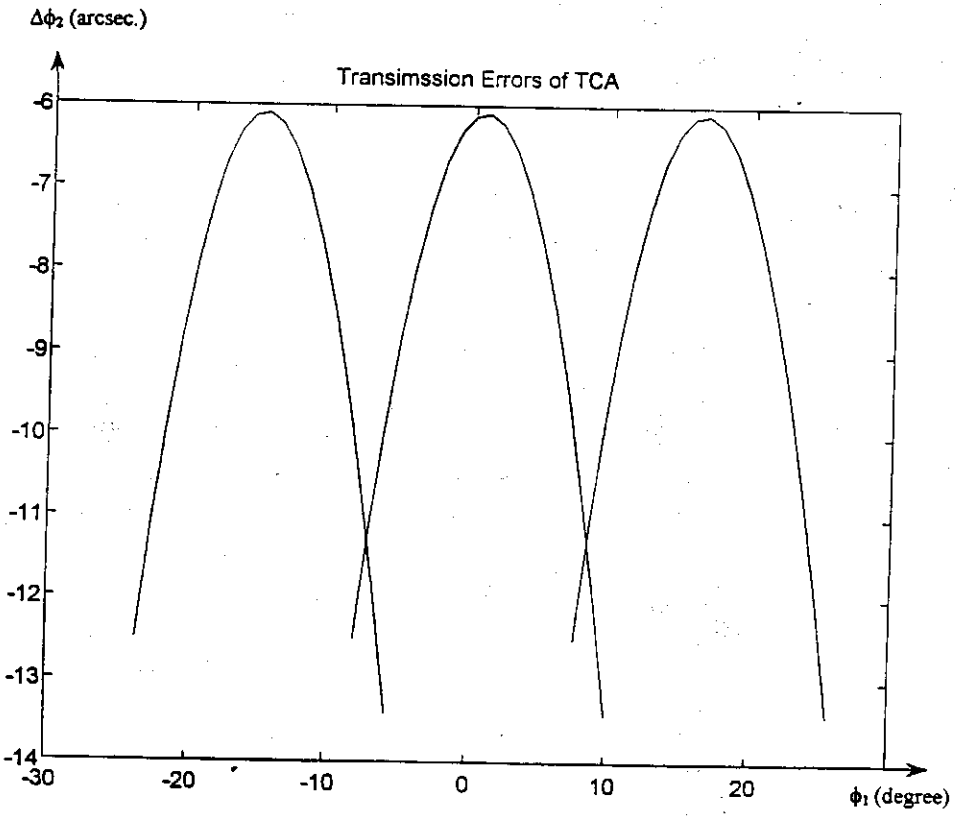

Fig. 17. Function of transmission errors $\Delta\phi_2(\phi_1)$ caused by $\Delta\lambda = 3$ arcmin; generation Case 2.

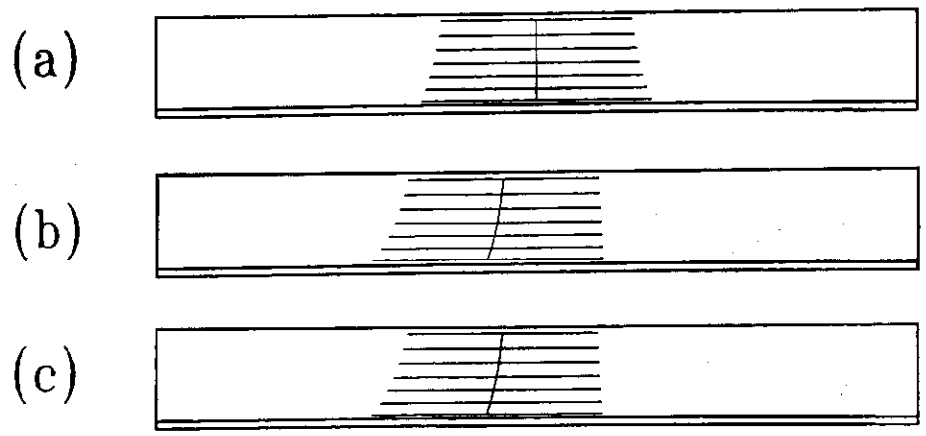

Fig. 18. Examples of bearing contact in misaligned gear drives: (a) $\Delta E = 0.1$ mm, (b) $\Delta\gamma = 3$ arcmin, (c) $\Delta\lambda = 3$ arcmin.

Case 2. Two rack-cutters with mismatched profiles are applied: a straight-line profile for the gear rack-cutter and a parabolic profile for the pinion rack-cutter (Fig. 7). Thus, profile crowning for the pinion tooth surface is provided. In addition, longitudinal crowning of the pinion tooth surface is provided by plunging of the pinion grinding disk.

Then we obtain that the pinion-tooth surfaces are in point contact at every instant and a parabolic function of transmission errors during the meshing is provided.

Figs. 13 and 14 show the functions of transmission errors obtained for case 1 for errors of alignment $\Delta\gamma = 3$ arcmin and $\Delta\lambda = 3$ arcmin. Functions of transmission errors are discontinuous ones and they may cause vibration.

The change of center distance as it could be expected for meshing of surfaces with involute profiles does not cause transmission errors.

Figs. 15–17 show functions of transmission errors caused by errors of alignment ΔE, $\Delta\gamma$ and $\Delta\lambda$, respectively. The obtained results confirm that a parabolic function of transmission errors is provided indeed.

Simulation of bearing contact: The determination of instantaneous contact ellipses needs the data on principal curvatures and directions at the contact point and the elastic approach δ [9] (taken for our computations as $\delta = 0.00025$ in.). The solution of this problem has been simplified by expressing the principal curvatures and the directions of contacting surfaces through the principal curvatures and directions of the tool generating surfaces [9]. The results of computation are represented in Fig. 18 and the drawings confirm that the bearing contact is localized and stabilized.

9. Stress analysis

Preliminary considerations: The goals of the stress analysis presented in this section are: determination of contact and bending stresses for two cases of design; asymmetric and symmetric spur gear drives, and comparison of stresses in both cases. The stress results presented in this paper are obtained using the finite element method [3,4,12]. These finite element results are obtained by using the general purpose finite element computer program ABAQUS/Standard 5.7 [1]. A PC version of this program running on Windows NT 4.0 operating system is used to obtain the numerical solution for the contact problem by nonlinear static analysis.

Two models of contacting teeth based on the real geometry of the pinion and the gear tooth surfaces have been developed. Since the PC version of ABAQUS does not have an interactive preprocessor, the CAD package I-Deas master series [6] is used for the development of geometric models and their meshing. The computations are performed for the asymmetric and symmetric spur gear drives with design parameters presented in Numerical example 1 and additional parameters taken as $\lambda_t = 1.5$ and $s_a = 0.05$ in.

One of the ABAQUS advantages in comparison with other FEA programs is that the ABAQUS can generate the contact elements automatically after the user appropriately defines the *contact pair* of surfaces

as the *master* and *slave* ones. The boundary conditions have been defined as follows: the nodes chosen on the gear tooth base are assumed to be fixed, and the contact of the pinion with the gear is obtained by turning the pinion about its axis.

Stress analysis of spur gears with symmetric tooth profiles was the subject of research presented in [2,11]. However, only one geometric model of the contact pair was used (for the pinion tooth) and the action of the other contacting tooth (of the mating gear) was simulated by application of a contact force to the pinion model. Therefore, the research performed in [2,11] could provide with good accuracy only the bending stresses in the root area.

Developed geometric models: The finite element models are shown in Fig. 19. The location of the contact point corresponds to Q_d (Fig. 7). A finer mesh for the two models is considered in the areas of concentration of stress, that are close to the tooth surfaces and the fillet areas. The fine mesh in such areas is obtained by setting an appropriate "*bias*" during the *mapped meshing* provided by I-Deas. First order brick elements are used in Global FE mesh. The total number of elements used is 1460 with 2172 nodes for each geometric model. The material of the model is steel with the properties of *Young's modulus* $E = 3 \times 10^7$ lbf/in^2 and the *Poisson's ratio* $\nu = 0.29$.

FEA: The models have been developed by I-Deas and then transferred to ABAQUS for stress analysis. The *master* and *slave* surfaces have been identified as the gear and pinion tooth surfaces respectively. Additional 24 internal elements and 48 nodes have been generated automatically in ABAQUS for contact elements. Two options related to the contact problem, "*small sliding*" and "*no friction*", have been selected.

The stress analysis has been performed for the following three cases:

Case 1. asymmetric spur gear drive with larger pressure angle 35°.

Case 2. asymmetric spur gear drive with smaller pressure angle 20°.

Case 3. symmetric spur gear drive with pressure angles for both sides 25°.

In each of these cases, the contacting models are assumed to have equal and opposite loads resulting from a torque of 250 Nm applied to the pinion.

Results of analysis: Figs. 20–22 show the contour plot of Von-Mises stresses. The numerical results are represented in Table 1.

The bending stresses obtained in the fillet of the contacting tooth side are considered as tension stresses, and those in the fillet of the opposite tooth side are considered as compression stresses.

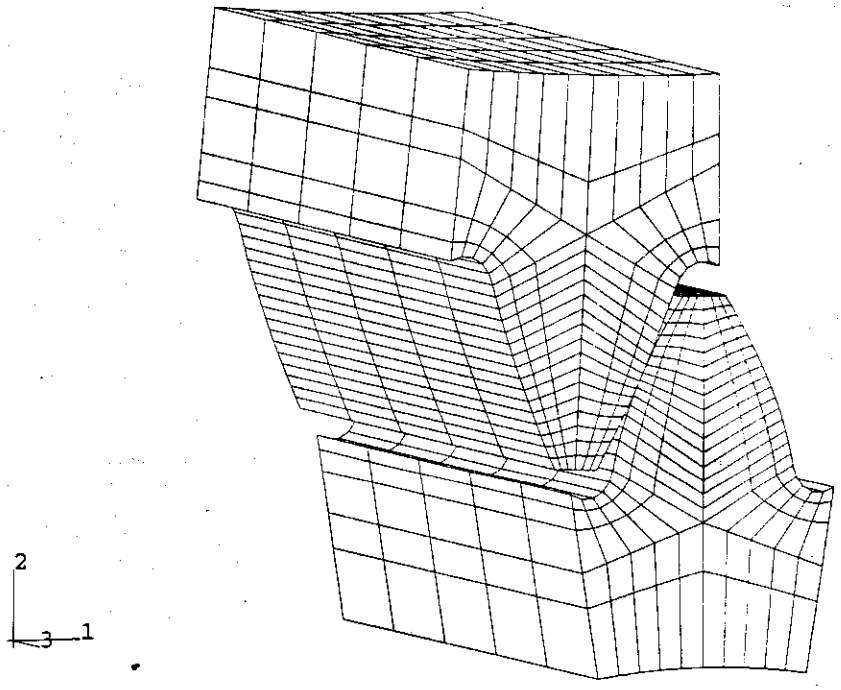

Fig. 19. Models applied for finite element analysis.

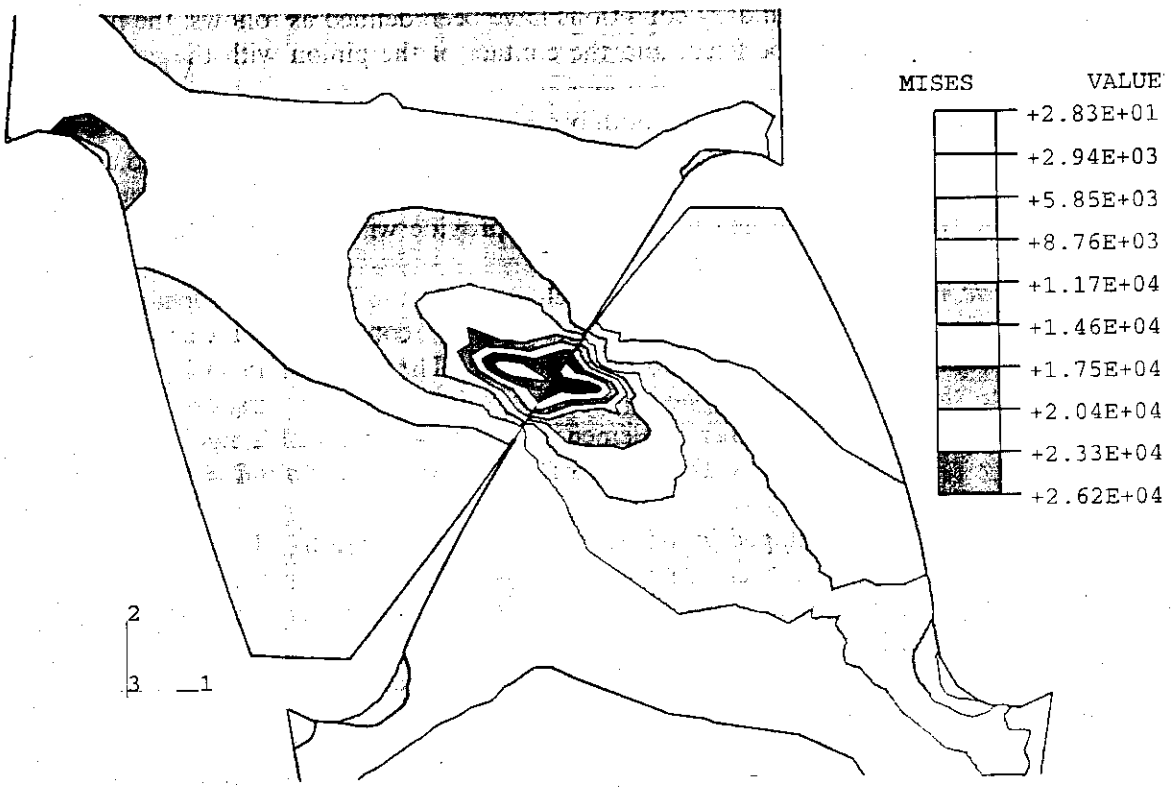

Fig. 20. Stress distribution in Case 1.

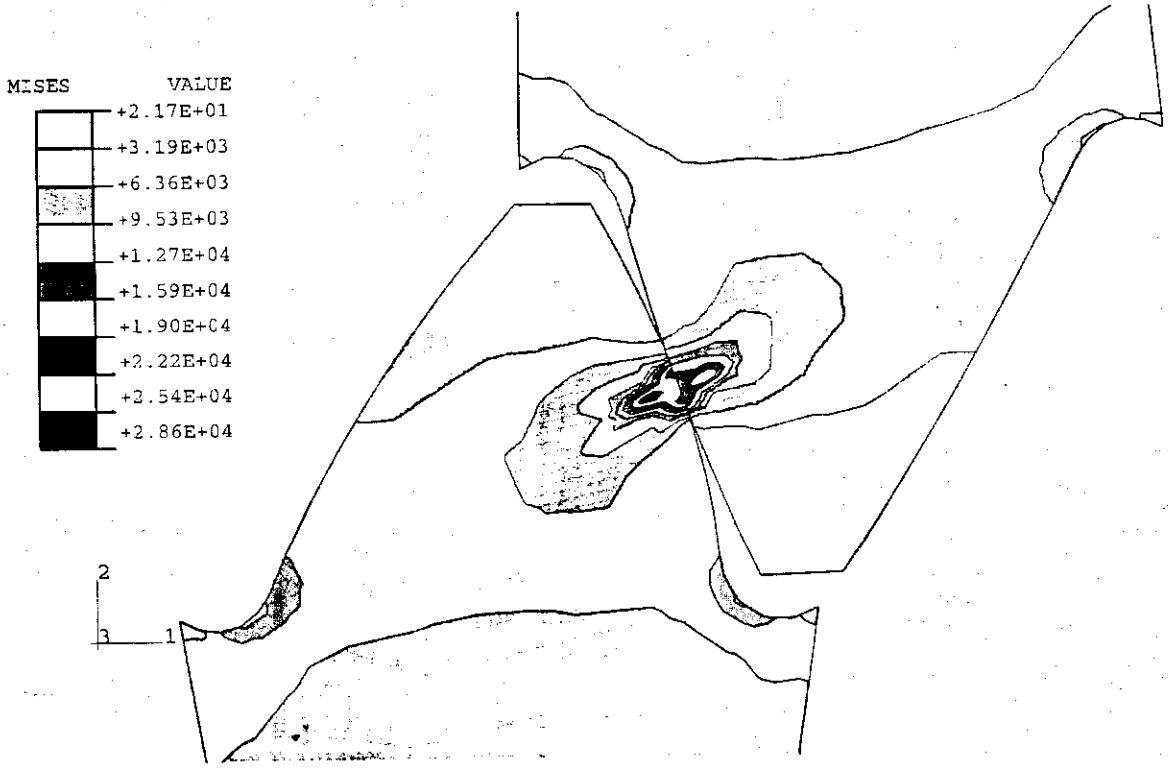

Fig. 21. Stress distribution in Case 2.

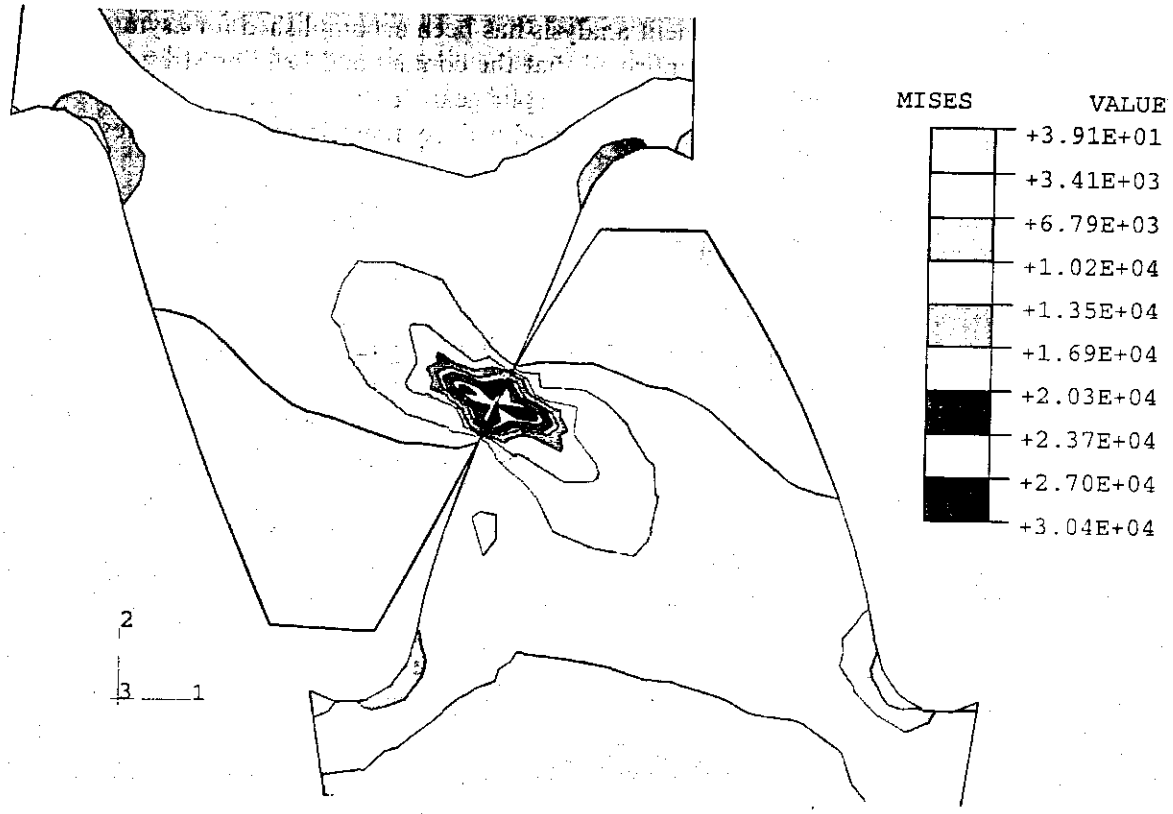

Fig. 22. Stress distribution in Case 3.

Table 1
Obtained pinion maximum Von-Mises stresses (in ksi units)

F.E. models	Contact stress	Bending stress (tension)	Bending stress (compression)
Case 1	26.2	8.7	14.6
Case 2	28.6	10.7	10.7
Case 3	30.4	10.2	13.5

Based on the obtained numerical results, the following conclusion can be made:

1. Maximum contact stresses are reduced by about 15% in Case 1 in comparison with Case 3. However, the contact stresses are reduced only by 6% in Case 2 in comparison with Case 3.
2. The tension bending stresses in Case 1 are 15% less in comparison with Case 3, but they are almost the same in Cases 2 and 3.
3. The larger pressure angle should be chosen for the driving side profiles.
4. Application of an asymmetric spur gear drive allows to reduce both stresses, the contact and bending stresses, by choosing the larger pressure angle for the driving side.

10. Conclusion

Based on the performed research, the following conclusions can be drawn:

1. Basic aspects of geometry of asymmetric involute spur gears have been represented (Sections 1–4).
2. Modified geometry of asymmetric spur gears for reduction of transmission errors and localization of bearing contact has been developed (Sections 5–7, Appendices A and B).
3. Simulation of meshing and contact of misaligned asymmetric spur gear drive has been developed (Section 8).

4. Stress analysis by application of finite element analysis has been accomplished for asymmetric and symmetric spur gear drives (Section 9). It is confirmed that the contact and bending stresses for the driving side (with a larger pressure angle) of an asymmetric spur gear drive are reduced.
5. Computer programs for the design and analysis of modified asymmetric spur gear drives have been developed.

Acknowledgements

The authors express their deep gratitude to the US Army Research Office for the financial support of this research project.

Appendix A. Pinion tooth surface equations

The pinion tooth surface is determined as the result of two enveloping processes: (i) in meshing of the pinion with the rack-cutter, when the intermediate pinion tooth surface $\Sigma_1^{(1)}$ is generated, and (ii) in the process of generation by a plunging disk, when the final, double-crowned pinion tooth surface $\Sigma_1^{(2)}$ is obtained.

Determination of $\Sigma_1^{(1)}$. The rack-cutter parabolic surface is represented in coordinate system S_c (Fig. 11). The rack-cutter and the pinion perform related translational and rotational motions as shown in Fig. 23. The pinion tooth surface $\Sigma_1^{(1)}$ is determined by the following equations.

$$\mathbf{r}_1^{(1)}(u_c, \theta_c, \psi_1) = \mathbf{M}_{1m}\mathbf{M}_{mc}\mathbf{r}_c(u_c, \theta_c), \tag{A.1}$$

$$f_1(u_c, \psi_1) = 0, \tag{A.2}$$

where (u_c, θ_c) are the surface parameters of the rack-cutter, ψ_1 is the generalized parameter of motion.

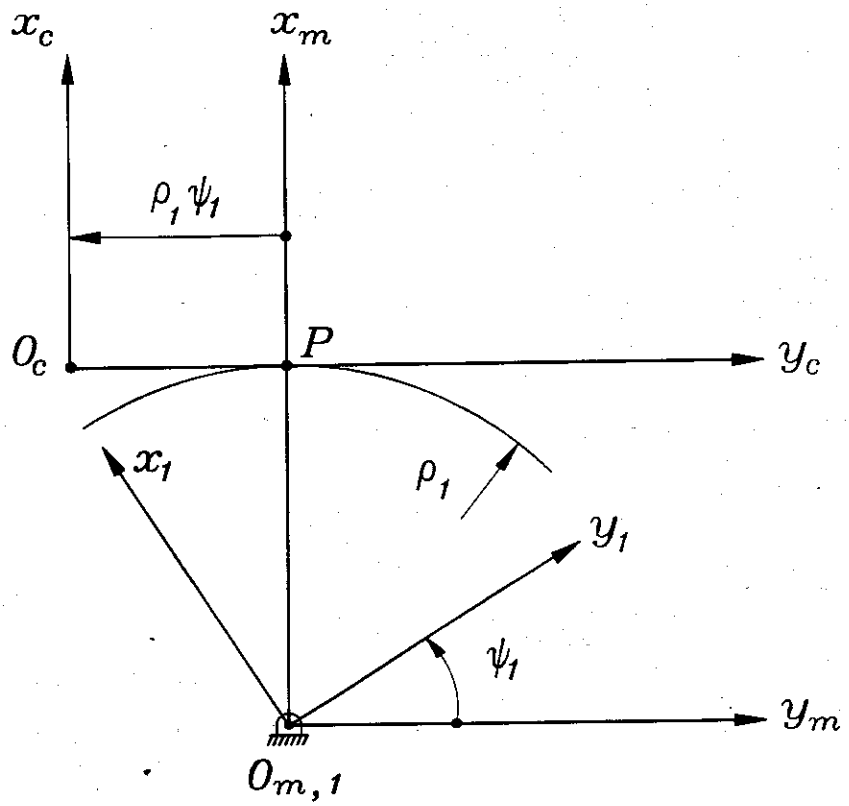

Fig. 23. Coordinate systems applied for derivation of pinion tooth surface.

Eq. (A.1) represents in S_1 the family of pinion rack-cutter surfaces. Eq. (A.2) is the equation of meshing that can be derived using the condition that the normal to the rack-cutter surface passes through the instantaneous axis of rotation P–P (Fig. 23). After derivations, we represent the equation of meshing as

$$f_1(u_c, \psi_1) = \rho_1 \psi_1 (2a_c u_c \cos \alpha + \sin \alpha) - \left(2a_c^2 u_c^3 - 2a_c u_c l_c + u_c\right) = 0. \tag{A.3}$$

Determination of double-crowned pinion tooth surface: After determination of pinion tooth surface $\Sigma_1^{(1)}$ it becomes possible to determine surface Σ_D of the pinion grinding disk. The axial section of the grinding disk is the same as the cross-section of pinion tooth surface $\Sigma_1^{(1)}$.

We apply for derivation of the double-crowned pinion tooth surface the following coordinate systems: S_1 and S_D that are rigidly connected to the pinion and the generating tool; the fixed coordinate system S_k (Fig. 24).

The generating disk performs during the process of generation: (i) translational motion along the z_k-axis, and (ii) plunging motion along the x_k-axis determined as

$$x_k^{(O_D)} = -a_{pl}\theta_k^2, \tag{A.4}$$

where θ_k is the displacement along the z_k-axis.

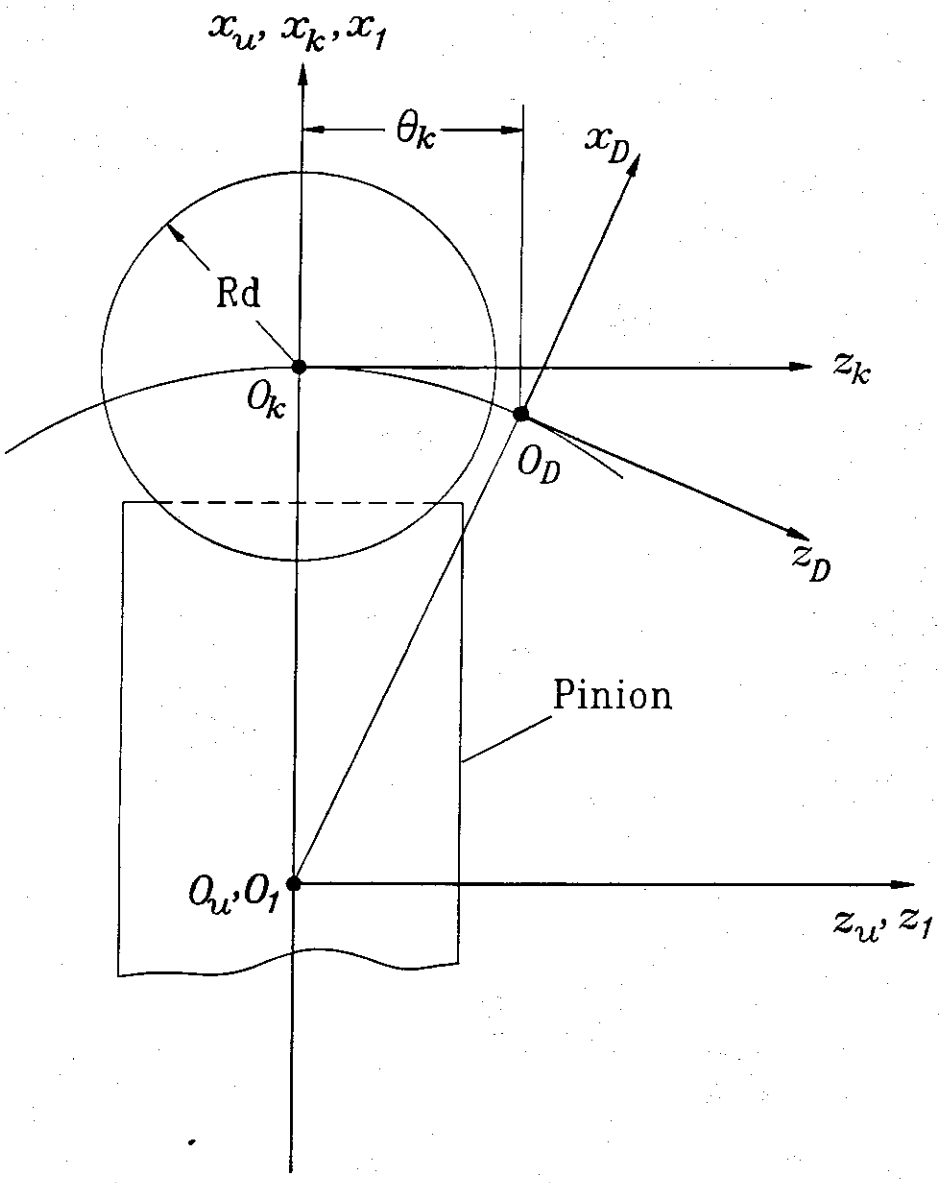

Fig. 24. Coordinate systems applied for generation of double-crowned pinion tooth surface.

The pinion tooth surface is generated as the envelope to the family of disk tool surfaces.

The derivation of double-crowned pinion tooth surface is based on the following procedure:

Step 1. We use an auxiliary coordinate system S_u which origin and axes coincide with the origin and axes of coordinate system S_k. We consider as known equations of profile crowned pinion tooth surface and represent them in coordinate system S_u.

Note: Coordinate axis x_u indicates the axis of pinion space while x_1 indicates that of the pinion tooth.

Step 2. We remind that the axial profile of the disk coincides with the axial section of the profile crowned pinion tooth surface determined as $z_u = 0$.

Step 3. We derive the disk tooth surface by rotation of its axial profile about the disk axis y_D. Then, we obtain the disk surface as

$$\mathbf{r}_D = \mathbf{r}_D(u_c, \theta_D). \tag{A.5}$$

Step 4. We represent the family of disk surfaces in coordinate system S_1 using the matrix equation

$$\mathbf{r}_1(u_c, \theta_D, \theta_k) = \mathbf{M}_{1k}\mathbf{M}_{kD}\mathbf{r}_D(u_c, \theta_D). \tag{A.6}$$

The equation of meshing may be represented as [9]

$$\left(\frac{\partial \mathbf{r}_1}{\partial u_c} \times \frac{\partial \mathbf{r}_1}{\partial \theta_D}\right) \cdot \frac{\partial \mathbf{r}_1}{\partial \theta_k} = f_3(u_c, \theta_D, \theta_k) = 0 \tag{A.7}$$

or as

$$\mathbf{N}_D \cdot \mathbf{v}_D^{(D1)} = f_3(u_c, \theta_D, \theta_k) = 0, \tag{A.8}$$

where $\mathbf{N}_D$ is the normal to the disk surface, $\mathbf{v}_D^{(D1)}$ the relative velocity of the disk with respect to the pinion. The subscript D indicates that vectors of Eq. (A.8) are represented in coordinate system S_D.

Eq. (A.6) and (A.7) or Eq. (A.8) considered simultaneously determine the envelope to the family of tool surfaces that is the double-crowned pinion tooth surface.

Fig. 25 shows the lines of contact between the disk and the pinion double-crowned tooth surface on the disk surface.

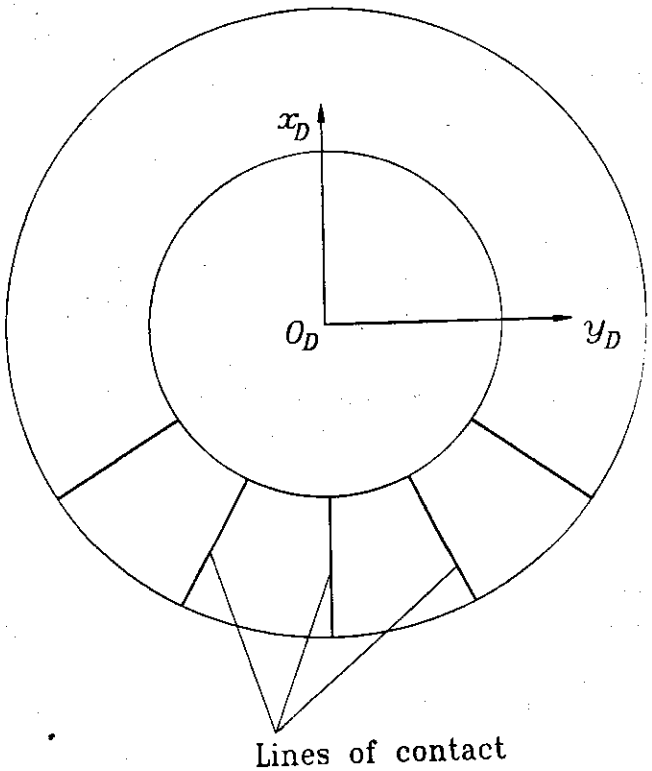

Fig. 25. Lines of contact on grinding disk.

Note: Vector of relative velocity of the disk is determined as the velocity of the disk in translation along axes x_k and z_k.

During the process of generation the disk performs rotation about the z_D-axis to provide the required magnitude of velocity of grinding (cutting). However, the disk rotation does not affect the mathematical determination of the envelope (pinion tooth surface) since the disk is a surface of revolution. Therefore, the rotation of the disk is ignored while the envelope is derived.

Appendix B. Gear tooth surface equations

The gear tooth surface is generated by a straight line rack-cutter. We use for derivations coordinate systems S_e and S_t that are rigidly connected to the rack-cutter, coordinate system S_2 that is rigidly connected to the gear, and the fixed coordinate system S_n (Fig. 26).

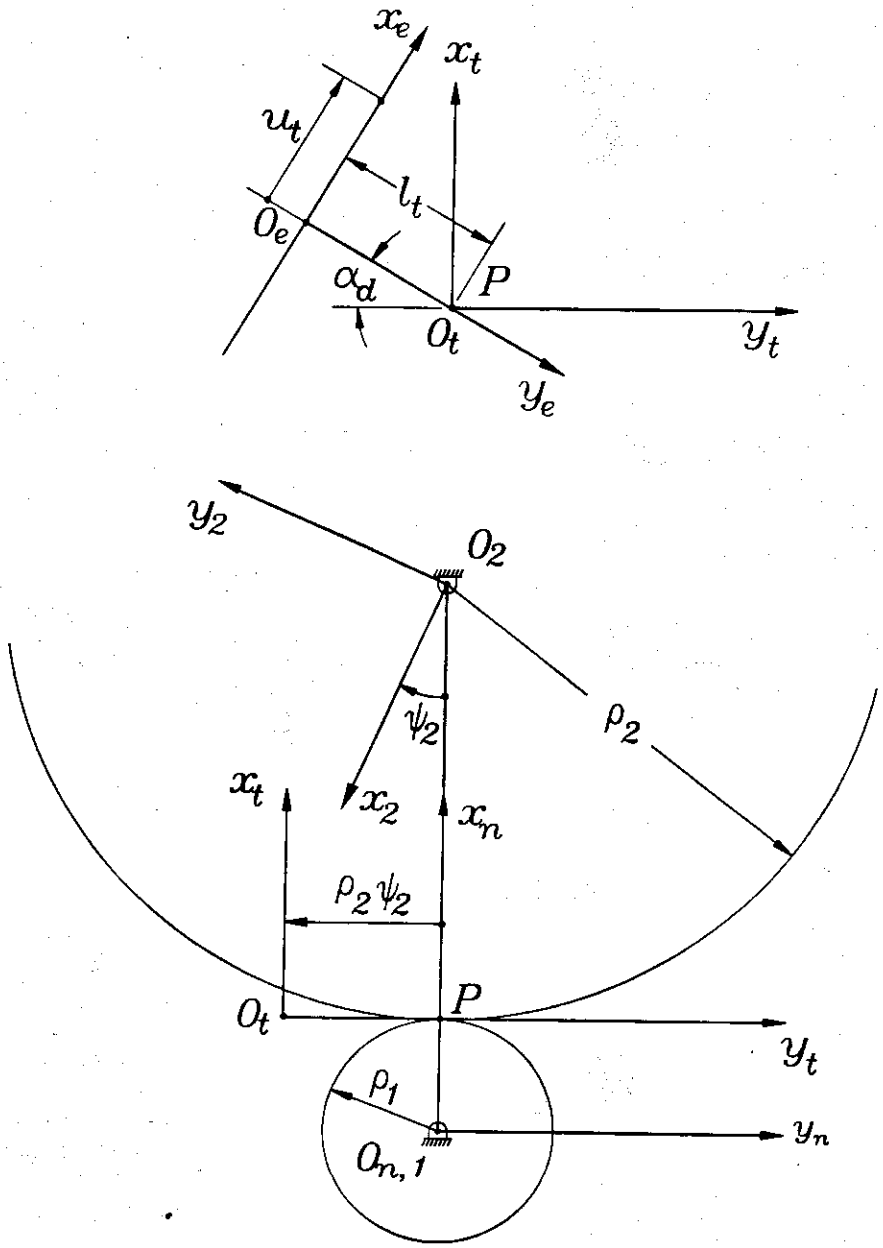

Fig. 26. Coordinate systems applied for derivation of gear tooth surface.

The rack-cutter surface Σ_t and its normal are represented in S_t by the following equations

$$\mathbf{r}_t(u_t,\theta_t)=\begin{bmatrix} u_t\cos\alpha_d + l_t\sin\alpha_d \\ u_t\sin\alpha_d - l_t\cos\alpha_d \\ \theta_t \\ 1 \end{bmatrix}, \tag{B.1}$$

$$\mathbf{N}_t=\mathbf{k}_t\times\frac{\partial\mathbf{r}_t}{\partial u_t}=\begin{bmatrix} -\sin\alpha_d \\ \cos\alpha_d \\ 0 \end{bmatrix}. \tag{B.2}$$

The family of rack-cutter surfaces is represented in coordinate system S_2 by the matrix equation

$$\mathbf{r}_2(u_t,\theta_t,\psi_2)=\mathbf{M}_{2t}(\psi_2)\mathbf{r}_t(u_t,\theta_t). \tag{B.3}$$

Equation of meshing is represented as

$$f_2(u_t,\psi_2)=\rho_2\psi_2\sin\alpha-u_t=0. \tag{B.4}$$

Eqs. (B.3) and (B.4) represent the gear tooth surface.

References

[1] ABAQUS/Standard 5.7 User's manual, Hibbitt, Karlsson & Sorensen.
[2] J.D. Andrews, A finite element analysis of bending stresses induced in external and internal involute spur gears, J. Strain Anal. 26 (3) (1991) 153.
[3] J.H. Argyris, Three-dimensional anisotropic and inhomogeneous media-matrix analysis for small and large displacements, Ingenier Archiv. 34 (1965) 33–35.
[4] J.H. Argyris, Energy Theorems and Structural Analysis, Butterworths, London, 1960.
[5] L. Hayer, Advanced transmission components investigation, Sikorski Aircraft division, USAAVRADCOM TR-82-D-11, 1986.
[6] I-Deas Master Series Manual, SDRC Part No. P-50002, Structural Dynamics Research Corporation.
[7] IMSL Math/LIBRARY: User's Manual, MALB-USM-UNBND-EN8901-1.1.2500, Citynest Bl., Houston, Texas.
[8] A.L. Kapelevich, Research and development of geometry of the modernized cylindrical involute gears, Ph.D. Thesis, Moscow Bauman State Technical University, 1984.
[9] F.L. Litvin, Gear Geometry and Applied Theory, Prentice-Hall, Englewood Cliffs, NJ, 1994.
[10] F.L. Litvin, Development of Gear Technology and Theory of Gearing, NASA Reference Publication 1406, ARL-TR-1500, 1998.
[11] V. Ramamurti, N.H. Vijayendra, C. Sujatha, Static and dynamic analysis of spur and bevel gear using FEM, Mech. Mach. Theory 33 (8) (1998) 1177–1193.
[12] O.C. Zienkiewicz, The Finite Element Method, McGraw-Hill, New York.